Title
Searching for the Decay of 229m Th

Author
Swanberg, Erik

Publication Date
2012

Peer reviewed|Thesis/dissertation

Searching for the Decay of ^{229m}Th

by

Erik Lars Swanberg Jr.

A dissertation submitted in partial satisfaction of the
requirements for the degree of
Doctor of Philosophy

in

Engineering - Nuclear Engineering

in the

Graduate Division

of the

University of California, Berkeley

Committee in charge:

Professor Eric B. Norman, Chair
Professor Edward C. Morse
Professor Heino Nitsche
Doctor Jason T. Burke

Fall 2012

Searching for the Decay of ^{229m}Th

Abstract

Searching for the Decay of ^{229m}Th

by

Erik Lars Swanberg Jr.

Doctor of Philosophy in Engineering - Nuclear Engineering

University of California, Berkeley

Professor Eric B. Norman, Chair

The existence of a low energy excited state in ^{229}Th was first postulated in 1975. The energy of the state was revised over the years from less than 100 eV in 1975, to 3.5 $\pm$ 1.0 eV in 1994, to 7.8 $\pm$ 0.5 eV in 2009, among others. Despite this progress, the decay of the state has never been observed, and the half life is unknown. While no measurement described in this dissertation was successful in these experiments either, many areas were searched and exclusion plots were produced. Measurements included looking for the internal conversion electron from the isomer, as well as any possible γ emission. $^{229\mathrm{m}}$Th was produced via the α decay of ^{233}U, and the recoiling ^{229}Th was collected on a catcher. Short time scales were probed using an α coincidence measurement that was sensitive from tens of nanoseconds to almost a millisecond. Intermediate time scales used a mechanical shutter that was sensitive from 2 milliseconds to a few seconds. Longer time scale measurements moved the catcher from the source to the detector, and were sensitive from a few seconds to a few days. The proper function of the system was confirmed by measuring $^{235\mathrm{m}}$U, which generated new results for the variation in its half life based on catcher material.

This dissertation is dedicated to my wife, my family, and friends.

Contents

List of Figures

List of Tables

Acknowledgments

Many people were involved in the experiments associated with this dissertation. Rick Norman was my advisor at Berkeley and was ultimately responsible for making it all possible. Jason Burke was instrumental in providing equipment, lab space, and knowledge, without which these experiments would never have happened. Robert Casperson was hugely helpful and was an indispensable sounding board throughout the process. Roger Henderson purified and prepared the ^{233}U, ^{234}U, and ^{239}Pu sources. Mau Chen provided calculations for the half life of the isomer via gamma, internal conversion, and bound internal conversion routes. Many other people helped in a variety of ways. Rather than try to name them all and inevitably forget some, I will just say thank you to all.

Chapter 1

Introduction

^{229}Th has the lowest known nuclear excited state at 7.8 $\pm$ 0.5 eV[1, 2]. This extremely low energy places any emitted γ rays in the ultraviolet region of the electromagnetic spectrum. It also allows for the possibility of exciting the ^{229}Th nucleus with a UV laser, low energy electrons, etc. The excited state is thought to be a relatively long lived isomer with a concomitantly narrow line width, so ^{229}Th could be used in a nuclear clock or as an extremely accurate probe of the constancy of the constants of nature. It should be an excellent tool to look for phenomenon such as Bound Internal Conversion (BIC), Nuclear Excitation by Electronic Transition (NEET), or Nuclear Excitation by Electron Capture (NEEC). After more than 35 years, the decay of ^{229m}Th has never been directly observed, and its half life is unknown. The experiments described here attempted to remedy this.

This dissertation begins by discussing previous experiments involving the 7.8 eV isomeric state, including the first indications of its existence, measurements of its energy and attempts to observe its decay and measure its half life. Previous theoretical studies are then briefly examined including its theoretical half life, possible excitation mechanisms, and uses. Chapter 2 develops the theoretical basis for the current work. Chapter 3 describes the experimental details. Chapter 4 relays the findings and results.

1.1 First Discovery and Energy Measurements

A low lying excited state in ^{229}Th was first proposed in 1976 by Kroger and Reich[3], with an energy estimated to be below 100 eV. They were investigating the structure of ^{229}Th via the α decay of ^{233}U and found a number of γ ray transition strengths that were consistent with a low energy $\frac{3}{2}^+$ band head for a rotational band they had found. See Figure 1.1. Additional experiments were conducted over the years to verify the existence of the state along with its energy, spin, parity, and Nilsson numbers. In 1990, Reich and Helmer used γ rays and known nuclear excited states to estimate the energy as -1 $\pm$ 4 eV[4]. Also in 1990, Burke et al. used the reaction ^{230}Th(d,t)^{229}Th to provide further evidence for the

state's existence[5]. The evidence included an angular distribution from the ^{230}Th(d,t)^{229}Th reaction that measured the spin and parity of the various states, yielding strong evidence for a rotational band based on a $\frac{3}{2}^+$ band head. A similar study was conducted previously but never published (see [5] for more details).

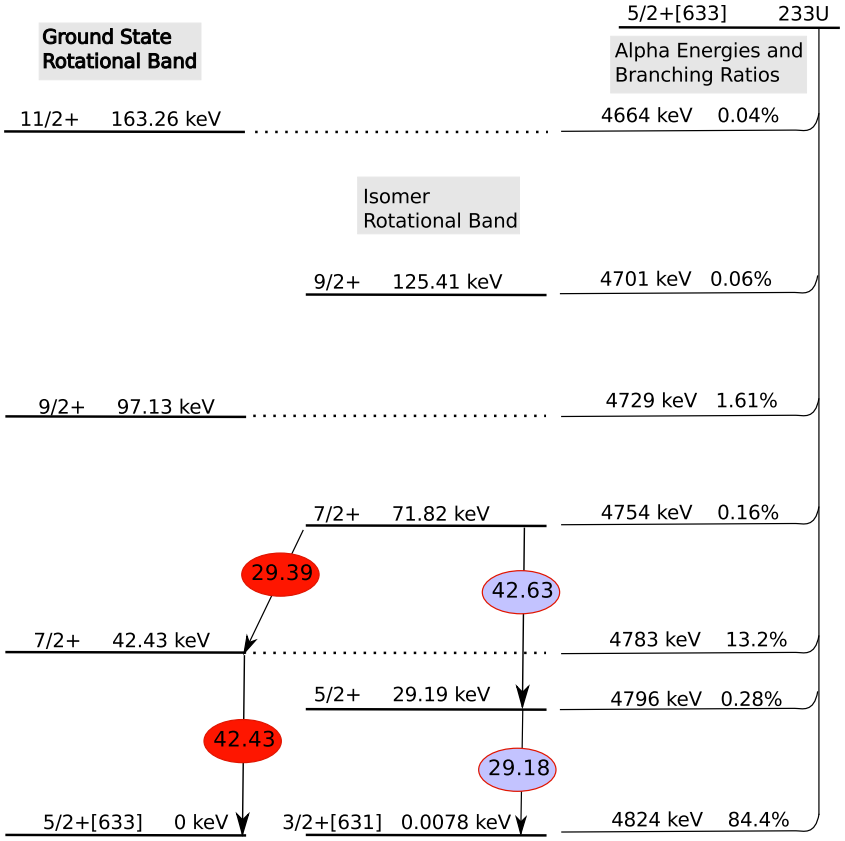

Figure 1.1: A partial level scheme for ^{229}Th. The γ transitions used in the experiment by Beck et al.[1] are highlighted. Also included are the branching ratios and energies of α decay from ^{233}U to the various levels, and the spin/parity and energy level of the states.

A new, more detailed γ ray study using HPGe detectors was conducted by Helmer and Reich in 1994. This experiment measured the energy as 3.5 $\pm$ 1.0 eV[6]. This paper was followed by two experiments that detected light of wavelengths consistent with a 3.5 eV decay. The first, in 1997, by Irwin et al. claimed to see UV and visible light from a ^{233}U source, which was attributed to the decay of ^{229m}Th[7]. Richardson et al. also claimed to see evidence of UV from the isomer, but from a liquid source dissolved in nitric acid[8]. They noted differences between their results and that of Irwin but felt they were probably still seeing the isomer. Two papers in 1999 tried to duplicate these positive UV results, but concluded the light seen was probably from excitation of nitrogen in air by α particles from the ^{233}U [9, 10].

A study of the level structure of ^{229}Th in 2003 by Barci et al. obtained a value of 3.4 ± 1.8 eV for the low lying state[11]. In 2005 Guimaraes-Filho and Helene reexamined the data from the 1994 Helmer and Reich experiment using a matrix system that included covariances in the analysis[12]. They obtained a value of 5.5 ± 1.0 eV for the isomer energy.

The latest measurement was made by Beck et al. in 2007 using a micro-calorimeter. They measured the energy level of the isomeric state as 7.8 ± 0.5 eV[2]. This measurement was possible because there are two γ ray cascades whose members are fortuitously close together in energy, both of which originate at the 71.82 keV state (see highlighted transitions in Figure 1.1). The first cascade consists of a 29.39 keV γ decay followed by a 42.43 keV γ decay to the ground state. The second cascade is a 42.63 keV γ decay followed by a 29.18 keV γ decay to the isomer state. Since there are two pairs of γ rays approximately 200 eV apart, the requirements for the absolute energy calibration are considerably relaxed while still yielding an accurate answer. The isomer energy level will be equal to the difference of the pairs of γ rays. That is

$$E_{\text{isomer}} = (\text{E}_{42.63} - \text{E}_{42.43}) - (\text{E}_{29.39} - \text{E}_{29.19}) \tag{1.1}$$

The calorimeter used had an energy resolution of approximately 26 eV Full Width at Half Maximum (FWHM), allowing for a very accurate determination of the differences. Care was taken to account for the interband transitions that alter the peak shapes and affect the energy determinations.

In 2009 a paper by Sakharov questions the energy and uncertainty measurements of most of the previous energy measurements[13]. He concludes the isomeric state, if it exists, is probably between 0 and 15 eV. Since the Beck measurement is the latest and most accurate, Sakharov's critical comments of it are worth repeating here. The most important appears to be that the statistical uncertainty in the energy of the peak with the fewest counts (the 29.19 keV peak), which Sakharov estimates is 300 counts, is 1.5 eV. This would clearly mean the uncertainty in the overall measurement is greater then 0.5 eV as published. While the point seems valid, it's unclear why the FWHM of the peak was used as the basis for the uncertainty calculation instead of the standard deviation (FWHM = 2.35σ). If the standard deviation of the peak is used the uncertainty would be 0.64 eV. If the standard deviation is used and the counts in the peak are 500 then the uncertainty is 0.5 eV, as published. The other main point Sakharov makes is the choice of contributions made to the peak by the interband branch, taken by Beck as 1/13, makes a large difference in the energy determined. If, instead of 1/13, the contribution is 1/4 as used by Barci[11], the energy is 9.3 eV. If it is 51% as used by Guimaraes-Filho[12] then the energy is 14.0 eV.

It is important to note that the decay from the isomer has never been directly observed. It is also important to note that, prior to the Beck measurement, it was thought the isomer had an energy below the ionization potential of thorium, making internal conversion impossible. The higher energy greatly changes the types of searches that should be conducted for the isomer and its half life. Since decays at low energies are usually dominated by internal

conversion, experimentalists started searching for electrons from the decay in addition to photons. Finally, the exact details of the decay will be complicated by many factors, including possible resonances in BIC decays, different lifetimes for neutral versus ionized thorium atoms, and differences in the atomic environment of thorium in materials.

1.2 Past Half-Life Experiments

Several different techniques have been used in the past to search for the isomer. The most direct measurements look for either photons or conversion electrons which are direct products of the isomer decay. Another approach is to look for a change in the α decay rate of $^{229g/229m}$Th caused by an increase in the number of the ^{229g}Th as the excited state decays to the ground state. One could also look for α energies that would be preferentially emitted by the excited state but not the ground state. Since ^{225}Ra frequently undergoes γ decay following the α decay of ^{229}Th, changes in the rate of γ emission could also indicate the decay of the excited state. These and other approaches have been tried at some point in the past and are briefly described here. The different experiments also generated ^{229m}Th in different ways.

In 2001, Browne et al. searched for the decay of the thorium isomer[14]. They separated thorium from a 25 gram ^{233}U sample, let fresh thorium grow in for 14.5 hours from the α decay of the uranium, and then separated the thorium again. The emission rate of 193.5 keV γ rays from the freshly separated thorium was measured using a High Purity Germanium (HPGe) detector. When the isomer decays to the ground state of thorium, the number of ground state thorium nuclei present will increase, which should change the total α decay rate, and hence γ ray emission rate. Their negative result suggests the half life is either less than 6 hours or greater than 20 days. This assumes the isomeric state does not α decay in the same manner as the ground state. While their paper does not discuss this, there are theoretical reasons to think the decay would be different. The details are discussed in chapter 2.

In 2003 Mitsugashira et al. created the isomer via the ^{230}Th$(\gamma, \mathrm{n})^{229}$Th reaction[15]. A bremsstrahlung source of either 22 or 30 MeV was used to irradiate the ^{230}Th target. They then measured the α decay of the ^{229}Th created. They predict the decay of the isomer would proceed preferentially to the 149.96 keV $\frac{3}{2}^+[631]$ state and the 42.77 keV $\frac{3}{2}^+[631]$ state in the radium daughter instead of the $\frac{5}{2}^+[633]$ state at 236.25 keV which the ^{229}Th ground state preferentially decays to. Decaying to a different energy level will measurably change the energy of the emitted α particle. They arrived at a half life of 13.9 ± 3 hours. As indicated by the large error on the measurement, the statistics were very low. In a 2005 paper, some of the authors of this paper said of this experiment: it appears "that the results contained interfering effects due to pile-up of the α-particles from ^{230}Th decay and β-rays of the other nuclear reaction products."[16]

In 2004 Moore et al. tried to measure the half life via UV photons that would be emitted by the (at the time) 3.5 eV isomeric state[17]. They used freshly produced ^{229}Th from a

200 mg ^{233}U source. Even though the experiment was carried out carefully, they were only sensitive to photons with a wavelength of 200 nm or longer, corresponding to about 6.2 eV. With the new energy measurement of 7.8 eV, they would not have been able to observe a direct γ decay of the isomer. It is possible they would have seen lower energy photons from recombination or other phenomenon, but they did not. They placed limits on the half life, assuming a 3.5 eV state populated by at least a 2% branching ratio from ^{233}U, at shorter than 5 minutes or longer than 115 days.

In 2005 Kikunaga et al. made ^{229m}Th via the reaction ^{232}Th(γ,p2n)^{229}Ac followed by β-decay[16]. They purified the actinium, then let thorium grow in, and then purified the thorium. The purified thorium was α counted about 5 hours after irradiation. While there were counts in the α spectrum in the energy region expected for ^{229m}Th, it was not clear if these counts were in fact from ^{229m}Th or if the counts came from a ^{228}Th impurity. Their results are therefore inconclusive.

Also in 2005, Kasamatsu et al. searched for the decay of the isomer by photon detection[18]. The process used was similar to Browne (see above). A source of ^{233}U was purified, allowed to decay to create ^{229}Th, then the thorium was purified and counted inside a quartz bowl with a Photo-Multiplier Tube (PMT). They ran the experiment twice, first with a grow-in time of 2 hours and an 18 minute chemical separation, and then with a grow-in time of 17 hours and a chemical separation in 30 minutes. The PMT used was sensitive to wavelengths between 170-650 nm (7.8 eV corresponds to 161 nm), but they discovered that the nitric acid solution, which the sample was disolved in, absorbs strongly in wavelengths below 340 nm. The authors conclude the half life is either less than 3 minutes or greater than 60 hours. Since the half life is expected to vary with chemical environment, they specify this range of half lives is for a nitric acid solution. They were also assuming the energy was near 3.5 eV, hence any signal could have been absorbed by the nitric acid solution.

In 2009 Inamura and Haba conducted an experiment where the half life was deduced to be between 1 and 3 minutes[19]. They claim to have excited the isomer in a hollow cathode via the nuclear excitation by electron transition (NEET) process. They changed their setup to measure possible half lives over a wide range of times. They claim a positive result when they ran the discharge for 5 minutes, pumped down the chamber to a vacuum, and then measured the α spectra. The statistics are poor, and it's possible that what they measured was an effect of pumping the chamber down, possibly due to α energy degradation by the gas remaining in the system. This result has not been confirmed.

Another measurement was attempted in 2009 by Kikunaga et al.[20]. They did a fast chemical separation of freshly prepared ^{229m}Th from a ^{233}U source. They were able to begin α counting within 15 minutes of elution of fresh thorium. They were unable to detect any difference between their measurement and that of regular ^{229}Th. This places a maximum limit on the half life of 2 hours.

The latest attempt was by Zhao et al. in 2012[21]. They claim to have seen a 6$\pm$1 hour decay from ^{229m}Th on a MgF_2 substrate using a PMT sensitive from approximately 160 nm to 270 nm. They did not see a decay using a PMT sensitive to 115 nm to 160 nm. As they

note, MgF_2 has a substantial afterglow after excitation from β or α particles, especially in the spectrum longer than 225 nm. They further note that a half life this long would indicate a γ decay with no internal conversion. Theoretically this is highly unlikely unless the isomer energy is significantly lower than the most recently measured value. The measures taken to subtract the background from the MgF_2 afterglow are too long to detail here. They note that the half life changes as the age of their ^{233}U source increases, probably due to interference from ^{232}U impurities, and the half life is also affected by the thickness of their sources. Their measured half life also disagrees with those found by others.

Despite repeated attempts to measure the half life, ^{229m}Th has not been conclusively observed to date. Repeated claims have been made of observations, but none have been confirmed. Several previous experiments have set limits on the half life as well.

1.3 Previous Theoretical Studies of ^{229m}Th

Several theoretical papers have been published on various aspects of ^{229m}Th. In 1998 Dykhne and Tkalya proposed using ^{229m}Th to verify the exponential decay law to 55 or 60 half lives, up from the current record of 45[22]. ^{229m}Th is useful for this application because of its (presumed) reasonable half life and extremely low energy. Tkalya has proposed using the isomer as the basis for a γ ray laser[23]. Several people have suggested using the isomer as a nuclear clock along with the closely related application of measuring any change in time of the fine structure constant[24, 25, 26]. Not everyone agrees the isomer would be good at measuring a change in the fine structure constant[27]. The possibility of BIC in ^{229}Th is discussed in [28, 29], and the idea of external conversion is described in [30]. Exciting the ground state ^{229}Th nucleus to form the isomer via either NEET or NEEC has been considered[31, 32]. Closer to the heart of the present experiment are the theoretical studies that have been performed on the half life of the isomer.

Several papers make predictions for the half life of the isomer. These calculations are complicated by several facts. The predicted half life depends on the energy, which was previously taken as 3.5 eV but is currently thought to be 7.8 eV. This greatly changes the effect of internal conversion. Another complication is the possibility of bound internal conversion (BIC), also known as resonant conversion, the electron bridge process, and inverse nuclear excitation by electronic transition (inverse NEET). It is also possible for conversion to occur with an electron from the substrate the thorium atom is in, termed external conversion (EC) here. In a thorium ion, the isomer no longer has enough energy for IC, and so the half life of the ion could be dramatically different.

In 1994 Helmer and Reich, in the same paper they announced their finding of the energy level in ^{229m}Th as 3.5 eV, calculate an estimate of the half life of the state[6]. They note a decay between the same two Nilsson states as the isomer in ^{233}U following β decay of ^{233}Pa. They use this decay as a model for the isomer decay, and find a half life of 45 hours for a 3.5 eV γ decay. They add that, since the uncertainty in their measurement is ± 1 eV, the

half life would be between 20 and 120 hours.

In 1999 Tkalya suggested that ^{229m}Th could decay nonradiatively via conversion with a conduction electron in a metal substrate[30]. It was assumed the state was at 3.5 eV and that internal conversion was therefore forbidden. While the new 7.8 eV energy measurement changes the conclusions, the points in the paper are still interesting. The most interesting point is to provide a means of decay which is virtually undetectable. In a nonradiative decay no photons would be produced, and the chances of a low energy electron escaping the material are small or, if the electron has an energy below the metal's work function, zero. The article derives an estimate of the cross section for electrons interacting with the nucleus and uses it to estimate the half life of a 3.5 eV isomer in a metal as 0.1 milliseconds. The model used treated the electrons as a gas.

Also in 1999 a paper by Karpeshin et al. discusses BIC for the 3.5 eV isomer[28]. They state that, since the electronic ground state of thorium is $(7s)^2(6d_{3/2})^2$, the most likely transition chains would be 7s-ns-$7p_{1/2}$ or 7s-ns-$7p_{3/2}$. This chain would be 3 orders of magnitude faster than γ decay or the chain $6d_{3/2}$-nd-$7p_{1/2}$. At 7.8 eV BIC is no longer applicable to the neutral atom, but these calculations are still useful for BIC in ionized atoms. They also suggest one of the 7s electrons in thorium is most likely to internally convert. This is reasonable since singly ionized thorium still has one of its two 7s electrons, and s orbital electrons are preferentially converted in IC due to their higher overlap with the nucleus.

In contrast to the above paper, a 2001 paper by Kálmán and Bükki argues the rates of γ decay and decay by BIC are approximately equal[29]. The contradiction with the 1999 paper by Karpeshin is broadly ascribed to a more accurate atomic model in the current paper. There is no discussion of substrate electrons, and again the energy was assumed to be near 3.5 eV.

In 2007 Karpeshin and Trzhaskovskaya wrote an article theorizing about internal conversion coefficients (ICC), Bound Inter Conversion Coefficients (BICC), photon spectra from the decay of the isomer, and half life estimates[33]. It's not clear why they use the electron binding energy, which they calculate as 5.2 eV, for calculations in isolated thorium atoms, where the proper value to use is the ionization potential (6.3 eV). Regardless, they find an ICC on the order of 10^9, and a BICC of about 600. They graph values for these numbers over a range of energies to make their work more broadly applicable to a range of energies of the isomer. Their predictions of emitted photon energies from BIC are primarily in the 1 to 2 eV range, corresponding to 620 to 1240 nm.

Ruchoswka et al.[34] studied the nuclear structure of ^{229}Th generated via the β decay of ^{229}Ac using $\beta\gamma\gamma$ triple coincidence measurements. They measured several M1 transition rates, allowing them to find B(M1) for the measured transitions. They also calculated B(M1) for these states, as well as the isomeric state, using the Quasi-Particle plus Phonon Method (QPPM). Their calculations generally agreed with the experimental values within a factor of 2. Since they were not able to measure the decay rate for the isomer, they estimated its half life using its calculated value for B(M1) of 0.025 μ_N^2. The half life is calculated using

the formula

$$t_{1/2} = \frac{10.95}{E_\gamma^3 B1(M)} \tag{1.2}$$

For 3.5 eV this yields a half life of 10^{+18}_{-5} hours. For a 5.5 eV state they calculate $2.6^{+2.2}_{-1.0}$ hours. Using their formula and an energy of 7.8 eV yields $0.92^{+0.18}_{-0.15}$ hours. Again, this is for decay via a photon with no IC or BIC.

Chapter 2

Nuclear Theory

This chapter serves as an overview of relevant nuclear theory and helps provide a common set of definitions and concepts. Much of the theory presented here follows the developments in Krane[35] and in Prussin[36]. It begins with a basic overview of nuclear structure, the spherical shell model, angular momentum, spin and parity, and the Nilsson model. This is followed by theoretical models of α decay, γ decay and internal conversion. The above concepts are then used to make predictions about the half life and decay mode of $^{229\mathrm{m}}$Th.

2.1 Basic Concepts and Definitions

There are several important concepts necessary to develop a rudimentary model of the atomic nucleus. The first is a nuclear potential, which is the attractive force which keeps the nucleons in the nucleus. The exact form is not important here, but is usually a function of radius (r), orbital angular momentum (ℓ), spin (s), and possibly an angular coordinate (θ or ϕ). Spin is often thought of as the intrinsic angular momentum of a particle, and is $\frac{1}{2}$ for electrons, protons, and neutrons. Non-spin angular momentum in a nucleus comes from orbital angular momentum and is an integer. The total angular momentum of a particle, which is the vector sum of s and ℓ, is j. The total angular momentum of the nucleus will be I, and is the vector sum of the angular momentum of the nucleons in the nucleus.

Parity indicates the symmetry of the wave function of a particle or system, and is represented by π. Positive parity indicates the wave function is symmetric about the origin, Ψ(r) = Ψ(-r) in spherical coordinates. Negative parity indicates the wave function is antisymmetric about the origin, Ψ(r) = -Ψ(-r). Letting positive parity be +1 and negative parity be -1, the parities are combined via the formula $\pi_{total} = \pi_1\pi_2\pi_3...$ The total angular momentum and parity are frequently used and indicated by I^{π}.

2.2 Nuclear Structure Models

2.2.1 Spherical Shell Model

The spherical shell model, as the name implies, assumes a spherically symmetric potential and shape for the nucleus; the nuclear potential has no dependence on θ or ϕ. The model makes many useful predictions that match experimental results well for many nuclei. In this model, neutrons and protons independently fill shells within the nuclear potential in order of increasing energy. The various orbitals have differing orbital angular momenta and parities, and differing projections of the angular momentum along the z-axis. The principal quantum number N, angular momentum ℓ, projection of angular momentum along the z-axis m_ℓ, and spin s are the quantum numbers used to describe the state of a nucleon.

While filling shells, the neutrons and protons pair with like particles such that their spins and angular momenta add to 0^+. Thus nuclei with even numbers of neutrons and protons have zero total angular momentum and positive parity ($I^\pi = 0^+$). In nuclei with one species even and the other odd, the odd particle determines the spin and parity of the nucleus based on its spin and the angular momentum and parity of the particular orbit it occupies. The primary nuclei used in this experiment are thorium, which has 90 protons; uranium, which has 92 protons; and plutonium, which has 94 protons. Thorium, uranium, and plutonium isotopes will either have I^π of 0^+ or a I^π determined by the odd neutron. The foregoing assumes ground state nuclei, or excitation of the odd particle only.

2.2.2 Nilsson Model of Deformed Nuclei

The Nilsson model has many similarities to the spherical shell model, but uses an ellipsoid of rotation for the nuclear shape and potential. It was developed because, especially in the region of $150 \leq A \leq 190$ and $A > 230$, the spherical shell model is not accurate. The non-spherical shape of nuclei can be inferred by the fact that their electric quadrupole moments are non-zero. The protons and neutrons still fill shells in the order of increasing energy, but the ellipsoidal shape causes energy degenerate orbitals in the spherical model to become non-degenerate. This is because nucleons with different m_ℓ will have different effective radii due to their angular orientation relative to the z-axis. See Figure 2.1. Both prolate and oblate ellipsoids are possible, and are distinguishable by the sign of their electric quadrupole moments. The quantum mechanical numbers used in the spherical shell model are not useful in the Nilsson model, and a new numbering system is used, $\Omega[Nn_z\Lambda]$. An example is $\frac{5}{2}[633]$, where the $\frac{5}{2}$ indicates the component of ℓ along the z-axis, and [633] are termed the asymptotic quantum numbers of the orbital, so called because they represent the quantum numbers of the state in a spherical nucleus. The first number is the principal quantum number N, the second is the number along the z-axis n_z, and the third is the angular momentum along the z-axis or Λ.

This model explains several features in the ^{229}Th nucleus. The most important is the

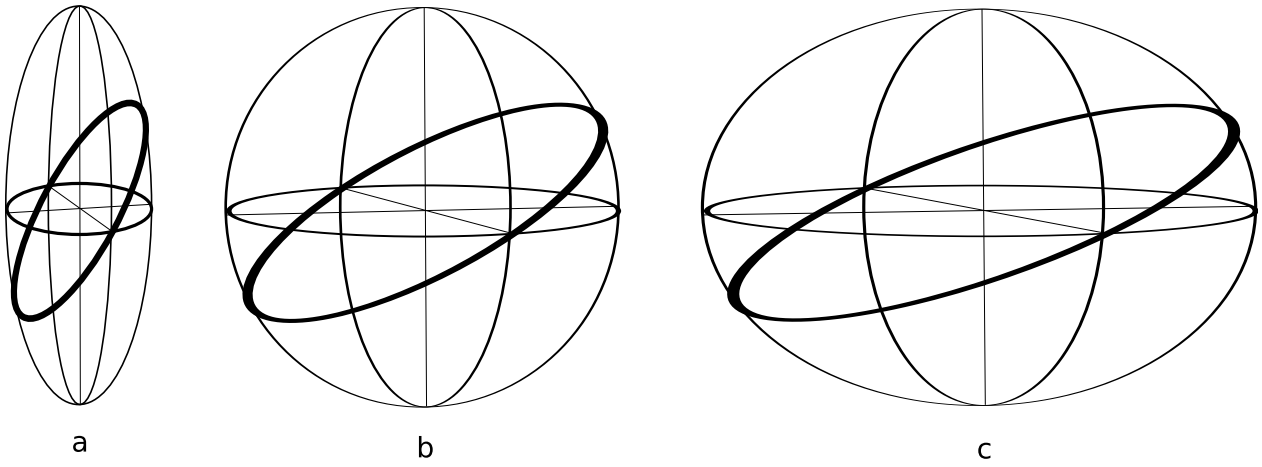

Figure 2.1: Examples of prolate (a), spherical (b), and oblate (c) ellipsoids of rotation used for the Nilsson model. An example nucleon orbital is included to illustrate how the average radius will change as the angle with the z-axis changes.

existence of the isomer itself, which comes from exciting the 139$^{\text{th}}$ neutron from one orbital to another. These orbitals would be energy degenerate in a spherical nucleus, and the isomer would not exist. Figure 2.2 shows the relative energies of the various orbitals derived from the Nilsson model, with the ground and isomer state of ^{229}Th highlighted. The amount of deformation in the nucleus is represented by ε_2. In this diagram for neutrons, the 126 in a circle indicates the number of neutrons at that point. ^{229}Th sits near where the $\frac{5}{2}$[633] and $\frac{3}{2}$[631] states cross. The ^{229}Th ground state is $\frac{5}{2}$[633] and the isomer is $\frac{3}{2}$[631]. Note that the model uses several adjustable parameters to fit the data, and Figure 2.2 hasn't been optimized for this particular region. This is why the valence neutron is predicted to be in the $\frac{3}{2}$[761] orbital instead of $\frac{5}{2}$[633]. The energy differences are so small that it's easy to imagine the $\frac{3}{2}$[761] actually being lower in energy than the $\frac{5}{2}$[633] and $\frac{3}{2}$[631] states, which would yield the correct result.

The measured electric quadrupole moment of ^{229}Th can be used to estimate the deformation of the nucleus. The deformation can then be compared with the point where the $\frac{5}{2}$[633] and $\frac{3}{2}$[631] states cross. The electric quadrupole of ^{229}Th is 4.3 $\pm$ 0.9 barns[38]. The following equations are used to calculate the Nilsson deformation parameter ε_2 from the electric quadrupole moment $\mathrm{Q_0}$

$$\mathrm{Q_0} = \frac{3}{\sqrt{5}\pi}\mathrm{R_{av}^2 z}\beta(1+0.16\beta) \tag{2.1}$$

$$\beta = \frac{4}{3}\sqrt{\frac{\pi}{5}}\frac{\Delta \mathrm{R}}{\mathrm{R_{av}}} \tag{2.2}$$

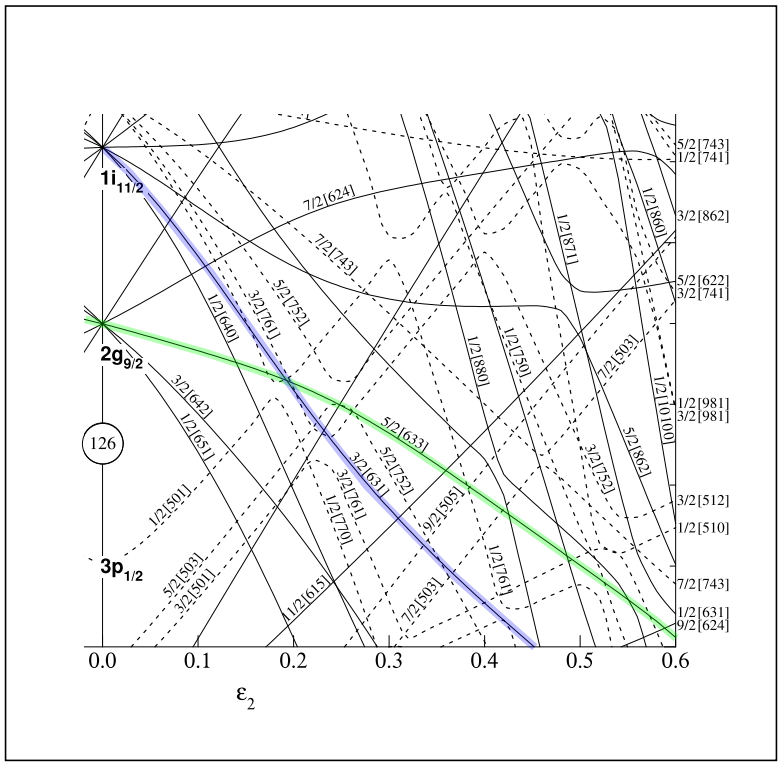

Figure 2.2: A partial Nilsson diagram for neutrons. The x-axis is a measure of how deformed the nucleus is, with positive being a prolate shape. The two highlighted lines are the ground (green or lighter) and isomeric (blue or darker) states of ^{229}Th. This figure is adapted from [37].

$$\varepsilon_2 = \delta + \frac{1}{6}\delta^2 + \frac{5}{18}\delta^3 + ... \tag{2.3}$$

$$\delta = \frac{\Delta R}{R_{av}} \tag{2.4}$$

The parameter β is used in calculations for the electric quadrupole, and is used as an intermediate variable in the above to find ε_2 from Q_0. Solving yields an ε_2 of 0.19 for ^{229}Th, which agrees very well with Figure 2.2. For comparison, the quadrupole moment of ^{233}U is $+3.663 \pm 0.008$ barns, which yields $\varepsilon_2 = 0.16$.

A unique property of deformed nuclei is rotational excitation. A spherical nucleus has a spherically symmetric wave function, which precludes rotation since all properties are independent of angle. A non-spherical nucleus, on the other hand, can have an observable rotation. Such rotational excitations are observed in a large number of nuclei and form characteristic bands. There are two rotational bands shown in Figure 1.1. The ground state

of ^{229}Th is the band head for one of the rotational bands and the isomer forms another band head. Notice that the angular momenta increase by one unit as the energy in the band increases.

2.3 Nuclear Decay Theory

Several different nuclear decay modes are important to predicting and measuring the ^{229m}Th half life, and important details of these are discussed in this section. Alpha decay is used to generate ^{229m}Th from ^{233}U. Gamma decay is one possible decay mechanism of the isomer, and can also be used to estimate the branching ratio of higher energy states in ^{229}Th decaying into the isomeric state. Internal conversion usually dominates γ decays at low energies, such as the isomer, and will be important to consider.

2.3.1 Alpha Decay

Alpha decay is the emission of an α particle from a parent nucleus. For a hypothetical parent nucleus X and daughter Y this is represented by:

$$ {}^{\mathrm{A}}_{\mathrm{Z}}\mathrm{X}_{\mathrm{N}} \rightarrow {}^{\mathrm{A-4}}_{\mathrm{Z-2}}\mathrm{Y}_{\mathrm{N-2}} + \alpha \tag{2.5} $$

The energy released, not including energy in excited states of the daughter or atomic ionization or excitation, is converted to kinetic energy of the daughter and α. The α particle gets approximately 98% of the energy, typically leaving the recoiling nucleus 80 to 100 keV. The kinetic energy T can be obtained by conserving energy and linear momentum, yielding

$$ \mathrm{T}_{\alpha} = \frac{\mathrm{Q}}{1 + \frac{\mathrm{m}_{\alpha}}{\mathrm{m}_{\mathrm{Y}}}} \qquad \text{and} \qquad \mathrm{T}_{\mathrm{Y}} = \frac{\mathrm{Q}}{1 + \frac{\mathrm{m}_{\mathrm{Y}}}{\mathrm{m}_{\alpha}}} \tag{2.6} $$

Q is the total energy available and may not be the Q-value of the decay. The mass of the α is m_{α} and the daughter mass is m_{Y}. A ^{229}Th nucleus produced by the alpha decay of ^{233}U will have a recoil energy of 84.3 keV, which is enough to escape from a source if the decay is near the surface. This experiment generates ^{229}Th from a ^{233}U source in this manner.

The charge state of the recoiling nucleus after α decay can vary considerably. Alpha decays to the ground state of the daughter typically yield recoiling nuclei with charges of +1 or +2 which quickly neutralize as they pass through material[39]. Thus many recoils escaping from a source will be neutral. Alpha decays to excited states present a different picture. High energy states will usually γ decay, which does not change the charge state. Low energy states typically strongly internally convert, leaving a vacancy in the electron shell of the atom. These vacancies can result in Auger electron showers. Gunter et al.[40] measured charge states up to +20 from the α decay of ^{226}Th which was followed by IC, with a peak at +10. Since almost 16% of α decays in ^{233}U are to various excited states, a wide

ℓ_α	Multiplier
0	1.000
1	0.846
2	0.608
3	0.373
4	0.196

Table 2.1: Angular momentum correction for ^{233}U α decay. The number in the second column is multiplied by the decay constant to improve accuracy. From Prussin[36]

range of charge states can be expected. A significant fraction of the isomer may come via excited states, and would likely be ionized as they leave the source.

The half life for α decay is frequently modeled assuming the α particle is already formed inside the nucleus and simply needs to tunnel out through the coulomb barrier. The frequency with which the α encounters the barrier, and the height and thickness of the barrier, can be used to calculate the half life. This is done in Krane[35] on page 253, with the result

$$t_{1/2} = 0.693\frac{a}{c}\sqrt{\frac{mc^2}{2(V_0+Q)}}\exp\left[2\sqrt{\frac{2mc^2}{(\hbar c)^2 Q}}\left(\frac{zZ'e^2}{4\pi\epsilon_0}\right)\left(\cos^{-1}\sqrt{\frac{Q}{B}}-\sqrt{\frac{Q}{B}\left(1-\frac{Q}{B}\right)}\right)\right] \quad (2.7)$$

Here a is the radius of the daughter nucleus plus the radius of the α particle, c is the speed of light, mc^2 is the mass and energy of the α particle, V_0 is the depth of the nuclear potential, Q is the energy available for the decay, and B is the height of the Coulomb barrier at a. This simple model ignores angular momentum and nuclear structure effects. It is adequate for making rough predications for branching ratios concerning ^{229m}Th.

An improvement takes into account the angular momentum of the α particle, ℓ_α, treating it simply as a centrifugal potential. This allows effects of differing angular momenta changes to be calculated by simply multiplying by a constant. The constants listed in Table 2.1 were used to incorporate the centrifugal potential in the calculations for the values in Table 2.2.

The α particle has $I^\pi = 0^+$ and will only carry orbital angular momentum. Conservation of angular momentum requires

$$|I_X - I_Y| \leq \ell_\alpha \leq |I_X + I_Y| \quad (2.8)$$

Conservation of parity requires states with the same parity to have even ℓ_α, and states with differing parity to have odd ℓ_α. Decays are potentially allowed with more than one ℓ_α. Decays via all routes must be considered to find the total decay rate.

Since it is not currently possible to measure the α branching ratio to the isomeric state of ^{229}Th directly, we can calculate it using the above model. Table 2.2 shows the results. The first four states listed in the table comprise the ground state rotational band. The second four are the isomer rotational band. To find the branching ratio one must determine what

State Energy (keV), I^+	Calculated Branching Ratio	Actual Branching Ratio	Calculated/ Actual
0, $5/2^+$	0.7529	0.8440	0.89
42.45, $7/2^+$	0.1708	0.1320	1.29
97.13, $9/2^+$	0.0706	0.0160	4.41
163.26, $11/2^+$	0.0058	0.0004	14.46
isomer, $3/2^+$	0.3355	N/A	N/A
29.19, $5/2^+$	0.4736	0.0028	169.14
71.82, $7/2^+$	0.1064	0.0016	65.29
125.41, $9/2^+$	0.0444	0.0006	74.00

Table 2.2: Calculated and observed branching ratios for α decay of ^{233}U. The first four states are the ground state and its rotational band, and the next four states are the isomeric state and its rotational band. Using the decay rate calculations for the ground state band, which are more accurate than the isomer band calculations, the calculated half life is 8710 years. The real half life is 159,200 years.

fraction of the total decay rate is due to that particular branch. This is easier using the decay constant, λ, rather than the half life. The two are related by

$$t_{1/2} = \frac{\ln(2)}{\lambda} \quad \text{and} \quad \lambda = \frac{\ln(2)}{t_{1/2}} \tag{2.9}$$

The half life can then be found from

$$t_{1/2} = \frac{\ln(2)}{\lambda_1 + \lambda_2 + \lambda_3 + ...} \tag{2.10}$$

The branching ratio for a particular state is given by

$$BR_1 = \frac{\lambda_1}{\lambda_1 + \lambda_2 + \lambda_3 + ...} \tag{2.11}$$

The decay rate calculations above do not consider the different nuclear structures of the ground state and isomer. In particular, the ground state of ^{233}U is $\frac{5}{2}^+[633]$, as is the ground state of ^{229}Th. The isomer, on the other hand, is $\frac{3}{2}^+[631]$ with a neutron in a different orbital. The difference makes it far less likely for ^{233}U to decay to the isomeric band than the ground state band, and so the calculations greatly overestimate the isomer branching ratios. Therefore only the ground state band's decay constants were used in calculating the half life of ^{233}U (Equation 2.10). For the same reason, the branching ratios in Table 2.2 were calculated using only the decay constants from the ground state band in the bottom of Equation 2.11. The calculated half life is 8710 years, too short by a factor of 18.

A potentially more accurate answer is found by comparing the actual branching ratios to the calculated branching ratios and finding the effect of the change in nuclear structure on the decay rates. The calculated branching ratios to the ground state and its first rotationally excited state are within 30% of measured values. States with higher angular momentum are not predicted as well. States in the rotational band of the isomer are significantly off, as expected due to the nuclear structure differences. A transition to the 29 keV level would have a different ℓ_α than the isomer, which is not very useful in predicting the branching ratio to the isomer. Transitions to the 71.82 and 125.41 keV states will both have ℓ_α predominantly of 2 and 4, just like the isomer, so these two states will be used to estimate the branching ratio to the isomer. Those two states' predicted branching ratios are an average of 69.6 times too high, presumably because their nuclear structure is different from the parent. Dividing the predicted branching ratio for the isomer by 69.6 yields a branching ratio of 0.48%. Since no experimental measurement of the branching ratio directly to the isomer exists, this can be used as a rough estimate.

In addition to the almost half a percent direct decay, the isomer can be populated by γ decays from higher energy levels. The amount is difficult to measure, but Barci et al.[11] estimate at least 2.1% of decays from higher energies pass through the isomer.

We also want to predict any difference in α decay between ground state ^{229}Th and the isomeric state. Several experiments have looked for the isomer via α decay, directly or indirectly[14][15][16][19][20]. The ground state of ^{225}Ra, the daughter of ^{229}Th, is $\frac{1}{2}^+$[631]. 56.2% of the time ^{229}Th decays to the 236.25 keV $\frac{5}{2}^+$[633] state, which is the same configuration as ^{229}Th. This can be viewed as the α particle leaving the nucleus with the odd neutron not changing states until after the α decay. There is also a 149.96 keV $\frac{3}{2}^+$[631] excited state in ^{225}Ra, which matches the $^{229\mathrm{m}}$Th configuration. We would expect, therefore, that the isomer would preferentially decay to this state, or one of it's rotational excitations. Since the energies and angular momentum changes are similar for the two routes, the α half life would likely be similar from the ground or isomeric state in ^{229}Th. The γ rays and α particles subsequently emitted, however, would be different. From the ground state, ^{229}Th emits an α at 4848 keV 56% of the time, which is the decay to the 236.25 keV $\frac{5}{2}^+$[633] state. It emits an α at 4930 keV 0.16% of the time, which is the decay to the 149.96 keV $\frac{3}{2}^+$[631] state. This ratio should change considerably in decay from the isomer. Similarly, the strongest γ from ^{229}Th α decay is the 193.5 keV line with a branching ratio of 4.4%. The isomer would decay instead to the $\frac{3}{2}^+$[631] state at 150 keV, and hence the 193.5 keV line would be greatly reduced. Conversely, the 107 keV line currently with a branching ratio of 0.8% would likely show an increase in strength in the decay from the isomer. Measurements to date have not detected the isomer by any of these changes.

2.3.2 Gamma Decay

Emission of a γ ray is one way a nucleus can rid itself of excess energy. We will use the Weiskopff model to predict the γ half life of ^{229m}Th. First, we will use the model directly. Then we will compare the Weiskopff estimates to known states in ^{233}U and ^{235m}U, and use these comparisons to improve the estimate for ^{229m}Th. Note that the actual decay will most likely be via internal conversion. The γ rate is estimated first since the internal conversion rate is calculated as a modification to the γ rate.

The Weiskopff model is based on the transition of a single proton from one nuclear shell to another, but it works as well for neutron transitions like those found in ^{229m}Th. The angular momentum ℓ_γ carried away by the γ is determined by the initial and final states of the nucleus, and must satisfy $|I_i - I_f| \leq \ell_\gamma \leq I_i + I_f$. Parity conservation and ℓ_γ determine the mulipolarity of the emitted γ ray. If parity doesn't change, electric multipoles are even and magnetic multipoles are odd. The situation is reversed if parity does change. For the ^{229m}Th γ transition from $\frac{3}{2}^+$ to $\frac{5}{2}^+$ the allowable transitions are M1, E2, M3, and E4. Lower order transitions typically dominate. For an M1 transition the half life is estimated as

$$t_{1/2} = \frac{2.20 \times 10^{-5}}{E^3} \tag{2.12}$$

which is 46.4 seconds for a 7.8 eV decay in ^{229m}Th. For an E2 transition

$$t_{1/2} = \frac{9.52 \times 10^{6}}{A^{4/3}E^5} \tag{2.13}$$

which is 2.35×10^{14} seconds for ^{229m}Th. The energy, E, is in keV. Some caveats for the Weiskopff model are that M1 rates are commonly hindered by 10 to 1000 times, and E2 rates in deformed nuclei (such as ^{229}Th) are enhanced by 10 to 100 times. Despite these caveats, the M1 decay will still dominate. Higher order transitions have even longer half lives. From this, the Weiskopff estimate for the half life of ^{229m}Th is between 46 and 46,000 seconds.

^{233}U has a $\frac{3}{2}^+[631]$ to $\frac{5}{2}^+[633]$ transition like ^{229m}Th, with an energy of 312 keV and M1 multipolarity. The Weiskopff estimate is 7.24×10^{-13} seconds, whereas the experimental half life is 1.2×10^{-10} seconds. This transition is hindered by a factor of 166, in line with the caveat above. Based on this, the ^{229m}Th half life should be 7691 seconds, or just over 2 hours. Recall from section 1.3 that Ruchoswka et al. derive an energy dependent decay rate which would yield a half life of 3312 seconds for a 7.8 eV decay[34]. This is the same transition used by Helmer and Reich to estimate a half life for a 3.5 eV γ decay of 45 hours[6]. The Weiskopff estimate with a hindrance factor of 166 yields a 3.5 eV γ decay of 24 hours.

As a last example, the Weisskopf estimate for the decay of the 76.8 eV decay in ^{235m}U is 2.41×10^{22} seconds. In reality, the decay proceeds via internal conversion with a half life of about 26 minutes. This shows how drastically internal conversion can alter decay rates at low energies.

2.3.3 Internal Conversion

Internal conversion (IC) occurs when a nucleus in an excited state gives its energy directly to an atomic electron, which is ejected from the atom. IC generally dominates γ decay at low energies and high multipolarities. The effect of IC is measured via an internal conversion coefficient α

$$\alpha = \frac{\lambda_{\mathrm{IC}}}{\lambda_\gamma} \tag{2.14}$$

where λ_{IC} is the IC decay constant and λ_γ is the γ decay constant.

The extremely low energy of $^{229\mathrm{m}}$Th causes simple models for computing α to fail for several reasons. First, the decay energy is an order of magnitude below what has been observed experimentally, and hence models have not been validated in this range. Also, it is usual for electrons in the K and L shells to dominate internal conversion processes. At the extremely low energies of $^{229\mathrm{m}}$Th and $^{235\mathrm{m}}$U only the outermost P and Q shell electrons have low enough binding energies to internally convert. Generally, α scales as $1/\mathrm{n}^3$, n being the principal quantum number of the electron, with P and Q corresponding to 6 and 7, respectively. This makes $^{229\mathrm{m}}$Th very different from more typical decays. Lastly, there may not be enough energy available to internally convert. If this is the case, it is still possible for Bound Internal Conversion (BIC) to occur. In BIC, an electron gains energy from the nucleus, but not enough to be ejected from the atom. Instead it jumps to a higher, bound, atomic state. This type of decay has only been seen in highly ionized tellurium[41].

Two estimates from more detailed models of the internal conversion process will be noted. The first is discussed in the paper by Karpeshin and Trzhaskovskaya[33] mentioned in Chapter 1, where α is roughly 10^9, and α_{BIC}, the bound internal conversion coefficient, is about 600. These numbers are used with the reservations stated in Chapter 1, but are almost certainly more accurate than simple models. Another model was used to calculate α by Mau Chen at Lawrence Livermore National Laboratory[42], with the result α is 1.95×10^9. The agreement between the two is somewhat reassuring. Unfortunately, Chen's α_{BIC} estimate is 4.88×10^6, which is significantly different. Both predict that IC will dominate if it's possible. Combining Chen's α with a γ half life of 7691 seconds (from the comparison with ^{233}U) yields a half life of 3.9 μs. Using the entire span of the Weisskopf estimate yields a half life from 24 to 24,000 ns. Chen also estimated α for $^{235\mathrm{m}}$U as 3.27×10^{20}. Combining this α with the Weisskopf estimate, the half life for $^{235\mathrm{m}}$U should be 73.7 seconds, about 21 times too short.

2.3.4 Low Energy Complications

There are two further complications that arise due to the low energy of the IC decay. First, the half life is expected to change based on the material the isomer is in. Second, converted electrons may not escape from the material to allow detection.

Low energy IC rates can be changed by the environment the decaying atom is in. As an example, the half life of ^{235m}U can vary by several per cent depending on the material the uranium atom is in. See for example [43][44][45], and the measurements of ^{235m}U made for this experiment in Table 3.2. The half life of an isolated ^{235m}U atom has never been measured, so no experimental evidence exists to say what the effect of a material is on the half life. The effect is expected to be much larger in ^{229m}Th because its decay energy is a factor of 10 lower.

The change in decay rate can be due to several different effects. One explanation is materials with higher electronegativity will pull electrons away from the thorium (or uranium) atom, reducing the transition rate. A relation of this type was shown in [44], where a plot of the half life of ^{235m}U versus the electronegativity for several metals is a nearly straight line.

The oxidation state of the thorium (or uranium) atom in the material can also change the half life. This was shown in [45], where the oxidation state of ^{235m}U was adjusted via two separate methods. In the first ^{235m}U was chemically processed into either UO_2, U_3O_8, or UO_3. In the second method, recoiling ^{235m}U nuclei were caught on a substrate of the same forms of uranium as in the first method. Both methods produced a change in half life, but the chemically processed method generated a much larger change. The lower oxidation states (+4) showed a shorter half life than higher oxidation states (+5 and +6). This implies that, with fewer electrons closely associated with the ^{235m}U atom, internal conversion proceeds more slowly. While the bonds in uranium oxides tend to be very ionic in nature, any bond type can be expected to change the decay rate.

Once the isomer decays, the converted electron will need to escape the material in order to be detected. The energy of the electron after it escapes from the material will be

$$T_e = E_{isomer} - E_{binding} - \phi \tag{2.15}$$

where T_e is the electron energy after escaping the material, E_{isomer} is the energy of the isomer, $E_{binding}$ is the binding energy of the converted electron, and ϕ is the work function of the material. This ignores any energy the electron looses as it travels in the material, which can be substantial. The binding energy and work function could easily exceed the decay energy in ^{229m}Th, precluding escape of the electron.

There are some options to increase the likelihood of the electron escaping. In semiconductors it is possible to have a negative electron affinity, meaning that any electrons in the conduction band will have enough energy to escape from the surface. If a converted electron makes it to the conduction band, it should escape. However, a recoiling thorium atom can potentially stop in any crystal lattice position in a material, and take on a range of oxidation states. This makes it difficult to predict the binding energy of converted electrons, where they might be in the energy band of a material, and if they will have enough energy to reach the conduction band. This argument is not restricted to semiconductors; it is difficult to predict the binding energy of the electrons of impurity atoms in any material. It is therefore difficult to predict which materials will be more likely to allow electrons to escape. For this

experiment a variety of likely candidates was tried, including metals, semiconductors, and insulators.

It is possible that the isomer will not have enough energy to internally convert. This appears to be true if the thorium atom is ionized. Even the +1 state has a ionization energy of 11.5 eV, higher than the isomer. Since recoiling thorium isomers will likely be ionized due to α decay and internal conversion from higher energy states, the isomer will not be able to decay in flight. Thorium with a high oxidation state in a material may similarly not be able to internally convert. If the state decays via BIC, then one would have to look for radiation from de-excitation of the atom. While this is possible, non-radiative recombination, where the energy is converted into phonons, will be a competing effect that may dominate.

Chapter 3

Equipment and Methods

This chapter describes how the experiments were conducted. It starts with a description of how the ^{229m}Th was obtained and some complications involved. The next section describes the sources used, including ^{233}U, ^{234}U, and ^{239}Pu. This is followed by a description of the catcher materials used, and then the detectors used and their electronics. With the groundwork complete the discussion moves to the different arrangements in which all the elements were combined to conduct the experiments. There is also a discussion of validation testing to make sure everything was working correctly.

3.1 Alpha Recoil Technique

The potentially very short half life of ^{229m}Th requires a constant source of the isomer. This experiment used the α decay of ^{233}U to produce ^{229}Th and ^{229m}Th. Since the recoiling ^{229}Th nuclei have on the order of 80 keV of kinetic energy, they can escape from a thin source. This method has been used in the past to study, for example, the half life of ^{235m}U[44]. Here it is called the Alpha Recoil Technique, or ART. All the measurements in this experiment use ART. Figure 3.1 shows the basic premise. Several different arrangements were used in order to cover the large range of half lives predicted for the decay of ^{229m}Th. While ART is straightforward, there are a few details to keep in mind.

The experiments were conducted in a vacuum to allow the recoiling Th to reach the catcher foils. The recoils will have varying energies and directions coming out of the source, which will allow them to penetrate the catcher to varying depths. After stopping in the catcher, decaying ^{229m}Th might emit electrons or photons which will need to escape from the catcher to allow detection. It was, therefore, important to select catcher materials that maximize the chance for electrons and photons to escape.

Recoiling nuclei can be positively charged as they escape the source (see §2.3.1). Further, α decays to low energy states in the daughter lead to internal conversion and a wide range of ionization states. The time for an 84 keV thorium recoil to travel 20 nm, a typical

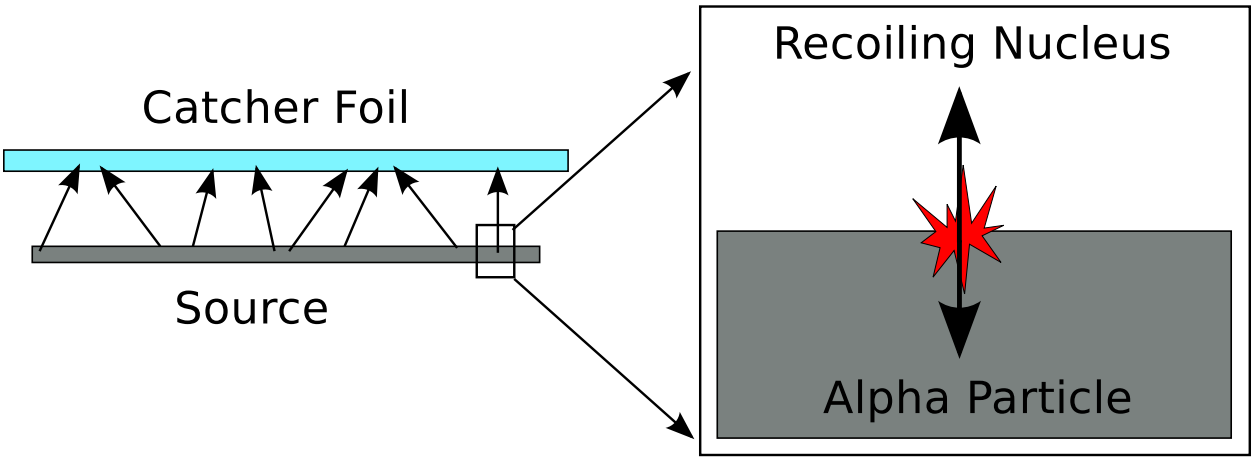

Figure 3.1: A diagram of the ART process. The star represents the nucleus undergoing alpha decay. If the source substrate is thick, the alpha particle will not escape through the back. For the thin mylar sources the alpha particles can penetrate the substrate and escape through the back with most of their original energy.

source thickness, is only 75 fs, whereas the decay time of the excited states is typically hundreds of ps. Even if an excited recoil is neutral when it exits the source, internal conversion can occur afterwards and ionize it. Any positively charged ^{229m}Th will have an ionization potential higher than the decay energy of the isomer. Since the gamma decay rate of ^{229m}Th is expected to be very much slower than internal conversion, ionized recoils would effectively be 'frozen' until they neutralize, presumably in a catcher foil or other material, when internal conversion would again become possible. This has implications when searching for half lives on the order of the time of flight of recoils.

3.2 Sources

The kinematics of α decay, as described by Equation 2.6, leaves the daughter nucleus with a significant amount of kinetic energy. If a source is prepared thin enough, then a large fraction of the recoiling daughters can escape the surface. The recoil escape efficiency, η_{recoil}, is defined as the number of recoils escaping from a source divided by the total number of α decays in the source. To design the source, η_{recoil} was estimated using the program Stopping and Range of Ions in Matter or SRIM[46]. SRIM results show that η_{recoil} starts to drop quickly once a ^{233}U source is roughly 20 nm thick, assuming a source composition of UO_2. Nève et al.[43] find a range of 10-15 nm for thorium stopping in gold, which is in good agreement with SRIM. A source thicker than this will not provide any additional recoils but can introduce background noise since α particles escape from much deeper in the source. Accordingly the sources used in this experiment were designed to be thick

enough to maximize the number of recoils without having excess activity which would cause background noise. This made it necessary to use large surface area sources to have reasonably high activities. SRIM was also used to predict η_{recoil} of ^{239}Pu and ^{234}U sources.

To validate the SRIM calculations, a measurement was made with a 3.3 μCi ^{233}U source. The source was placed in a vacuum chamber 2 mm from a collector for 2 weeks. The collector was larger than the source to make sure all the escaping recoils were collected. The collector was then α-counted with a Si detector for 3 weeks. η_{recoil} for the source can be determined from the activity of ^{229}Th on the collector, A(^{229}Th), along with the source activity A(^{233}U)

$$\eta_{\text{recoil}} = \frac{\text{Number of } ^{229}\text{Th on catcher}}{\text{Number of } ^{233}\text{U decays}} = \frac{\text{A}(^{229}\text{Th})/\lambda(^{229}\text{Th})}{\text{A}(^{233}\text{U}) \cdot \text{Collection Time}} \tag{3.1}$$

Figure 3.2 shows the resulting α spectrum, including the ^{232}U daughters as well as the ^{229}Th peak of interest. The source and collector were α-counted in the same geometry, so the detection efficiency cancels out.

The measured efficiency was 37.8±5.5%. This means 37.8% of ^{233}U decays in the source result in a recoil on the catcher. Because the actual composition of the source was unknown, SRIM was run with different compositions including UO_2, U_3O_8, UO_3, $UO_2(NO_3)_2$ (uranyl nitrate), and metallic uranium. The predictions from SRIM varied from 12% for uranyl nitrate to 31% for uranium metal. The measurement suggests the uranium was in a metallic form. This is possible if the uranium in solution was reduced to the metallic form during electroplating and deposited on the aluminum substrate. Similar measurements for ^{239}Pu and ^{234}U are impractical due to the long half life of their daughters, ^{235}U and ^{230}Th. Instead SRIM results for metallic ^{239}Pu and ^{234}U were used where needed.

The ^{233}U used in this experiment was originally made at the MIT nuclear reactor a few decades ago. A ^{232}Th target was irradiated with neutrons, creating ^{233}Th which beta decays twice to produce ^{233}U:

$$^{232}\text{Th}(\text{n},\gamma)^{233}\text{Th} \xrightarrow[22.3\,\text{min},\ \beta^-]{} {}^{233}\text{Pa} \xrightarrow[27\,\text{days},\ \beta^-]{} {}^{233}\text{U} \tag{3.2}$$

Within a year the ^{233}Pa has almost entirely decayed to ^{233}U, which has a half life of 159,200 years. The only contaminants found in this experiment were ^{232}U and the daughters of both ^{232}U and ^{233}U. The decay chains for ^{232}U and ^{233}U are shown in Figure 3.3. Because of the half lives in the decay chain, the ^{232}U daughters build up to unacceptable levels quickly, primarily for the moving catcher arrangement. Therefore the source material needed to be purified before production of the sources.

To remove the daughter impurities, the material was dissolved in an 8M nitric acid solution and put through an anion exchange column which preferentially captures thorium, which will be the major impurity, and lets uranium pass. The product was dried and then dissolved in 9M hydrochloric acid, which was passed through another anion exchange column. Here the uranium was captured while other elements passed. After rinsing with additional

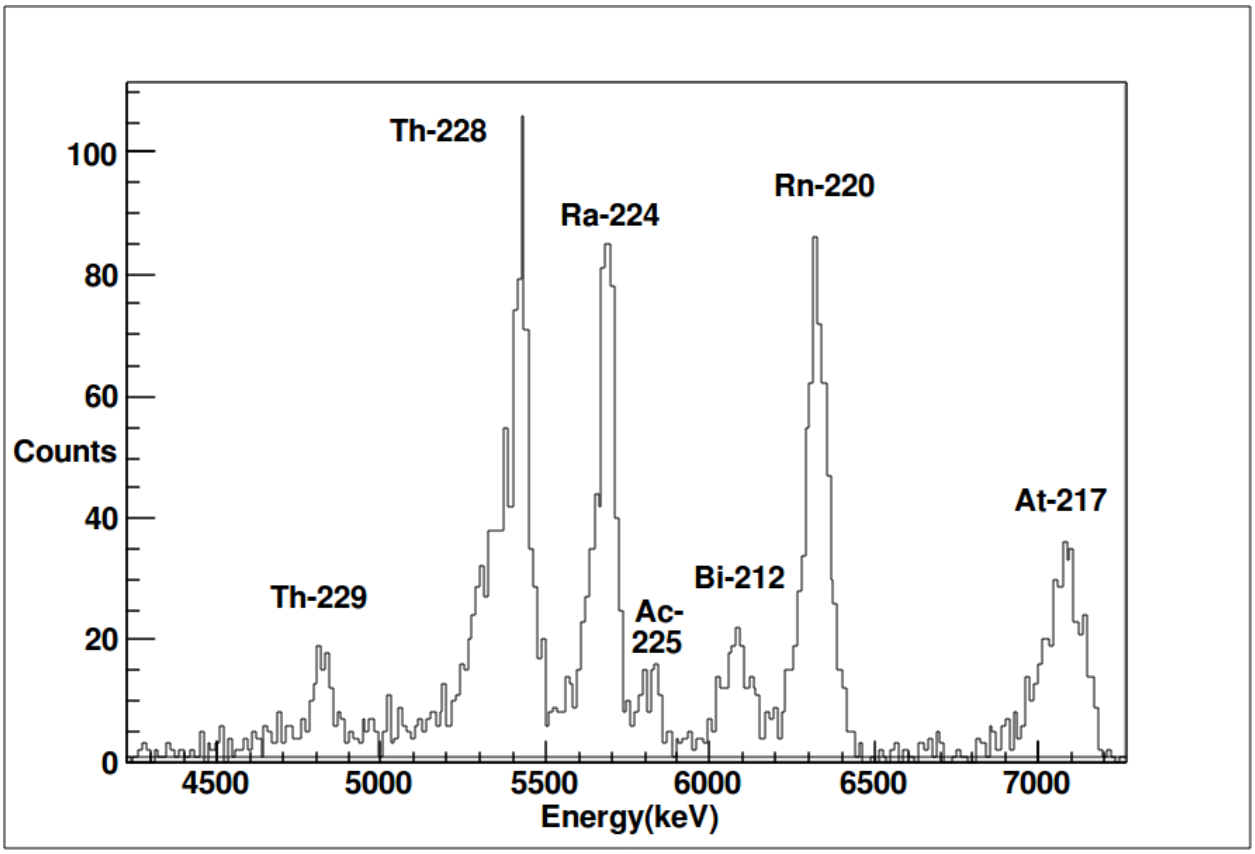

Figure 3.2: This is an α energy spectrum of the catcher that had collected recoiling nuclei from a 3.3 μCi ^{233}U source for two weeks. The α measurement lasted 3 weeks. The ^{229}Th can be seen on the left. Other peaks are daughters either from ^{229}Th (odd A) or from the ^{232}U contaminant (even A).

9M hydrochloric acid to remove impurities, the uranium was eluted with 1M hydrochloric acid. This was dried and dissolved in a small amount of nitric acid. Finally, the nitric acid solution was added to alcohol, which was the liquid used to electroplate the sources.

All the sources were α counted to determine their activities and the activities of any impurities. The activities of the sources used are shown in Table 3.1. The only impurity immediately after purifying was ^{232}U, which cannot be separated chemically. The ^{232}U activity is 0.05% of the ^{233}U activity, corresponding to 0.22 parts per million on a per atom basis. Since the half life of ^{232}U is 68.9 years, the ratio of ^{232}U to ^{233}U was constant during the experiment. The daughters of both ^{232}U and ^{233}U build up with time. The first daughter of ^{233}U is ^{229}Th which builds in very slowly due to its 7932 year half life. The first daughter of ^{232}U, ^{228}Th, has a 1.9 year half life and builds in much more quickly. The ingrowth rate of ^{228}Th was 0.02 Bq/day/μCi of ^{233}U. These slightly odd units are useful since the sources are

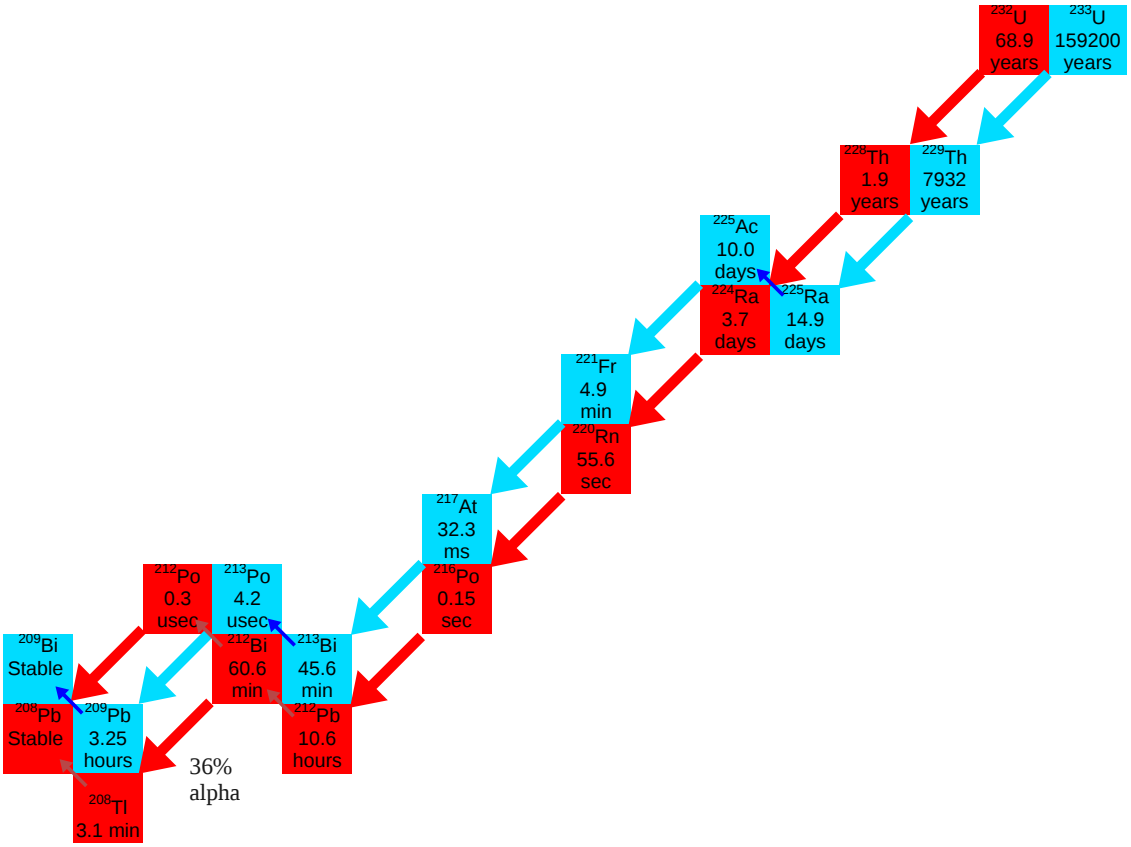

Figure 3.3: The decay chain for ^{233}U and ^{232}U. Note the wide range of half lives, from 300 ns to 1.9 years. Note also that very few recoils from β decay will leave the surface. The recoil energy after a β decay is typically less than 20 eV in a heavy nucleus, and the recoil energy distribution, like the β particle energy distribution, will extend to zero.

noted by their ^{233}U activity, not their ^{232}U. For the slow half life measurements ^{228}Th and its daughters cause an increased background. Once the catcher is no longer exposed to the source the daughters decay away, causing the background to decay which interferes with the search for the decay of the isomer. Figure 3.5 shows an energy spectrum of a ^{233}U source a few months after preparation. The major impurities have been identified.

Larger sources, between 2 and 15 μCi, were electroplated onto eighth inch thick aluminum squares in 2 inch diameter circles. See Figure 3.4. Initial sources were non-uniform, which is bad since the thicker source areas will be too thick to allow recoiling atoms to escape efficiently and areas of low concentration will have less useful material than they could. A better electrode was made for electroplating, and subsequent sources were much more uniform.

Smaller 0.2 μCi sources, 3 of ^{233}U and 1 of ^{234}U, were electroplated onto thin aluminized

Thick Sources			
Material	Activity (μCi)	Half Life	Notes
^{233}U	3.86±0.06	159,200	Design activity 4 μCi #1
^{233}U	3.288±0.055	159,200	Design activity 3.5 μCi #2
^{233}U	11.77±0.18	159,200	Design activity 10 μCi
^{234}U	3.555±0.058	245,500	Design activity 4 μCi
^{239}Pu	5.384±0.086	24,110	Design activity 2 μCi
^{239}Pu	11.065±0.17	24,110	Design activity 10 μCi
Thin Sources			
Material	Activity (μCi)	Half Life	Notes
^{233}U	0.157±0.0043	159,200	Design activity 0.2 μCi #1
^{233}U	0.146±0.0041	159,200	Design activity 0.2 μCi #2
^{233}U	0.122±0.0082	159,200	Design activity 0.2 μCi #2 Backwards
^{233}U	0.223±0.0055	159,200	Design activity 0.2 μCi #3
^{234}U	0.164±0.0042	245,500	Design activity 0.2 μCi
^{241}Am	0.113±0.0013	432.17	Used for efficiency calibration
			Activity and error from source calibration sheet

Table 3.1: Several sources used during the experiment are listed here. The ^{233}U was used as a source of ^{229m}Th. The ^{239}Pu was used as a source of ^{235m}U. ^{234}U was used as a control to compare to the ^{233}U source. ^{241}Am was a NIST traceable source used for efficiency calibrations. One of the thin sources was measured backwards to see how much energy the α particles loose traveling through the mylar (180 keV). Based on the activity from the forward and backward direction, a small fraction of the α particles are probably scattered as well.

mylar supported by an aluminum frame. The source area is 0.5 inches in diameter. The α particles can penetrate the mylar source substrate while only loosing 180 keV. One of these sources is visible in Figure 3.15.

As previously mentioned, ^{233}U sources were used to produce ^{229}Th and ^{229m}Th. ^{239}Pu sources were used to produce ^{235m}U, which is useful for testing the system since it has the next lowest known nuclear decay energy at 76 eV and internally converts with a 26 minute half life. ^{234}U was used as a control since there are no isomeric states in its decay chain and it has similar properties to ^{233}U, namely a half life of 245,500 years compared to 159,200 years for ^{233}U and a primary alpha energy of 4774.6 keV compared to ^{233}U at 4824.0 keV.

3.3 Catcher Materials

The materials that the recoiling nuclei are collected on are called catchers. Several different catcher materials were utilized. Metals were used with varying properties, including electronegativity and work function. Previous experiments [43][44][45] have shown that the

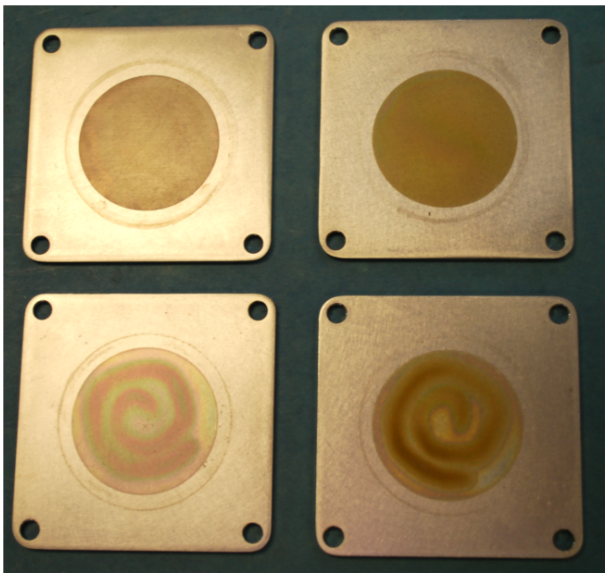

Figure 3.4: A Picture showing two ^{233}U sources, on the right side, and two ^{239}Pu sources on the left. Note the spiral on the bottom two sources. A different electrode was designed for the electroplating process, which resulted in the much more uniform sources shown on top.

^{235m}U decay rate changes based on these properties, so a wide variety of these properties could be useful while looking for the half life of ^{229m}Th. Semiconductors were also used. These included some materials traditionally considered insulators, but which have a definite band gap. Examples are SiO_2 (quartz), MgF_2, and Al_2O_3 (sapphire). Several amorphous materials were tried as well, including teflon and acrylic. See Table 3.2 for more details. Of note when searching for photons, MgF_2 is transparent between 120 and 8000 nm, and Al_2O_3 is transparent between 160 and 5300 nm. This should allow for detection of potential γ rays at 7.8 eV, which corresponds to 161 nm. It will also allow any electronic transition or capture radiation to be detected after the decay.

Since the thorium isomer has such a low energy, there is a concern that converted electrons will not be able to escape from the catcher material. For this reason, materials with low work functions were tested in addition to more traditional materials.

3.4 Detectors

Three main types of detector were used. The first are Multi-Channel Plate (MCP) detectors, used to detect individual electrons. The second type are surface barrier silicon detectors, or Si detectors, used to detect and measure the energy of alpha particles. Lastly are photomultiplier tubes (PMT), used to detect single photons.

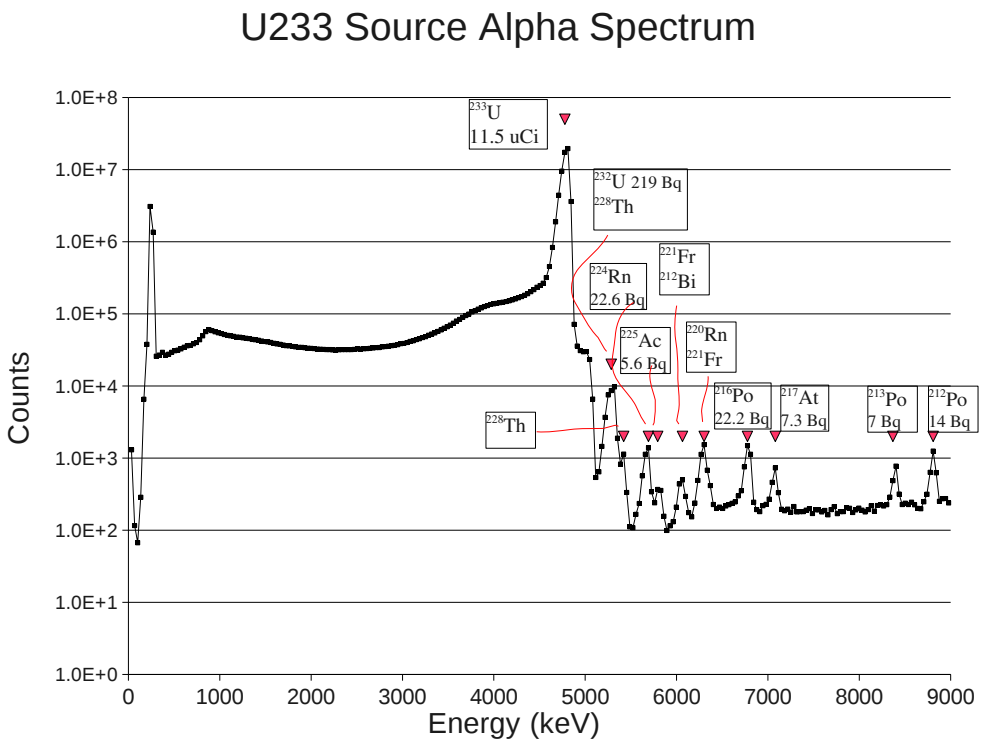

Figure 3.5: This is an alpha spectrum of a ^{233}U source. Contaminants are indicated. Since most contaminants are daughter products, they build in over time.

3.4.1 Multi-Channel Plate Detectors

Multi-Channel Plate detectors, or MCPs, can be used to detect electrons or ions. They can have gains of 10^7 or more. They consist of many small (about 10 μm) channels in a substrate with a high electric field applied. Electrons enter a channel, collide with the wall and cause several more electrons to be emitted. These are then accelerated down the channel by the electric field and the process is repeated. Figure 3.6 shows the MCP layout used. Note the two separate sections of the MCP. A single electron entering a channel can saturate the channel with electrons by the end of the first section. The small gap between the first and second sections allows electrons to spread to several channels and continue the amplification process.

The high voltage for the different layers are supplied via a resistive voltage divider network. Figure 3.7 shows the circuit and voltages biased according to the manufacturers specifications, which were not necessarily those actually used. The divider network allows one high voltage power supply to generate the 4 required voltages, which greatly reduces the risk of accidentally applying an incorrect voltage and damaging the MCP. The grid was biased to +2000 volts with respect to ground, to accelerate incoming electrons. The front of

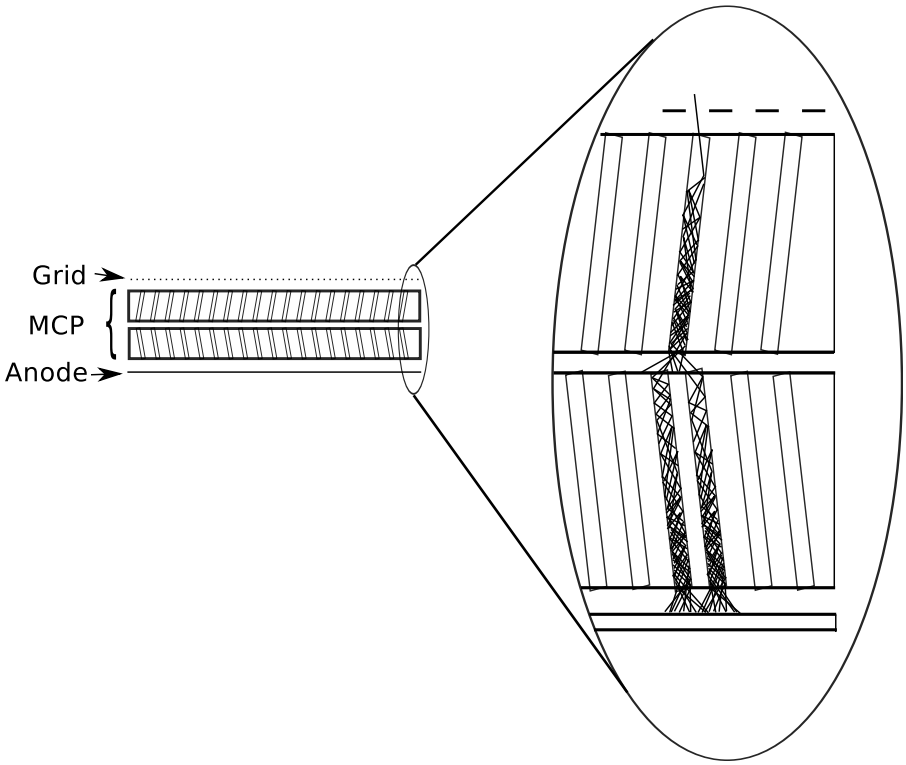

Figure 3.6: A diagram of the Multi-Channel Plate (MCP) detector. The top is a metallic grid biased slightly negative to the front surface of the MCP to reflect electrons back to the MCP. There are two MCP layers to allow greater multiplication of electrons. The bottom anode is a solid metal surface that collects the charge.

the MCP was about 150 volts more positive than the grid, which helps to recapture electrons that otherwise might have bounced off the front MCP surface. There was another 2000 volts across the MCP itself. The anode collects the charge generated by the MCP and was at 150 volts more positive than the bottom of the MCP, or about +4300 volts total. The MCP efficiency for detecting electrons is over 70 per cent for electrons with 2 keV energy[47]. This is higher than the channel area of MCPs, indicating electrons that hit the front face are indeed returned to the system and detected.

A typical output pulse from the MCP is 100 mV, negative going, and 10 ns wide. The amplitude varied considerably between pulses due to the random nature of the multiplication process. This should not be construed as an energy measurement of the incoming particle. The FWHM rated by the manufacturer is 70%. Also the electrons were accelerated from nearly zero energy to 2 keV. The voltage across the MCP was adjusted to allow rejection of noise while measuring the actual electrons. The signal went to an Ortec VT-120A non-inverting 20X preamplifier with a 350 MHz bandwidth. This fed either an edge sensing discriminator (for moving catcher and mechanical shutter measurements) or a constant

fraction discriminator (CFD) (for the alpha coincidence measurements).

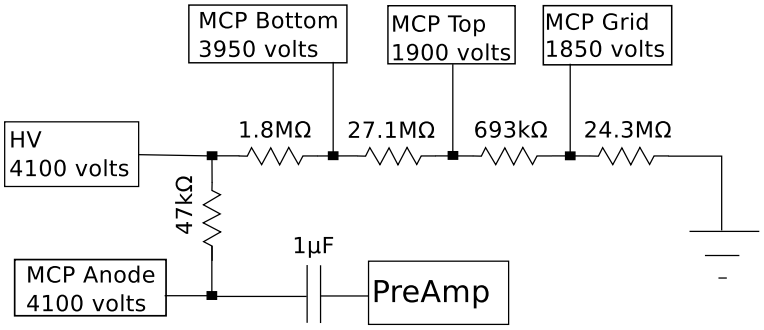

Figure 3.7: A schematic of the resistor divider network used to provide the 4 voltages required to operate the MCP. The 47 kΩ anode resistor prevents the high voltage power supply from overwhelming the MCP signal from the anode. The 1μF capacitor blocks the high voltage DC while allowing the signal to pass to the preamplifier. The voltages listed assume the resistors are exactly at their rated values and yield a voltage across the MCP in line with the manufacturers ratings. During the experiment the voltage was adjusted to provide a good signal to noise ratio, which was slightly higher then the manufacturers ratings.

3.4.2 Silicon Surface Barrier Detectors

Silicon Surface Barrier Detectors, or Si detectors, are used to detect alpha particles. They consist of a layer of doped silicon with electrodes on the faces, configured like a large diode. A reverse bias is applied to the diode to create a large intrinsic volume. When an energetic particle enters the intrinsic volume it creates electron-hole pairs which are collected at the electrodes. The number of pairs created is proportional to the energy of the incoming particle, assuming the particle comes to rest in the detector. This allows an energy spectrum to be taken of a sample. If the detector is calibrated with an appropriate source, the activity of the measured sample can be determined. Figure 3.15 has a picture of a silicon detector, and Figure 3.5 shows an alpha spectrum of a ^{233}U source acquired with a silicon detector. Energy resolution is on the order of 20 keV FWHM. The resolution is degraded for α particles passing through a mylar layer due to energy straggling.

The Si detectors were biased at 185 volts, and used a standard preamplifier and an Ortec research amplifier. The Si signal was much slower than the MCP signal: typically 100 μs wide out of the preamp and 20 μs wide after shaping in the research amp. The slow response presents no problem for α spectroscopy, and a leading edge discriminator was used. The α coincidence measurements require timing resolution better than 10 ns. A CFD was used which provided the necessary timing resolution. The signals were digitized with an Ortec AD413 8,192 channel ADC.

3.4.3 PhotoMultiplier Tubes

An Electron Tubes 9426 PhotoMultiplier Tube (PMT) was used to detect light emitted either as a γ ray or from electronic rearrangement. PMTs have a gain of 10^6 or more, which enables them to detect individual photons. The ET9426 has a 2 inch diameter MgF_2 window and is sensitive from 115 to 600 nm. The output signals were relatively fast at about 20 ns wide. The signal was fed to a VT120A non-inverting 20X preamp and then into a discriminator, either leading edge or, for the α coincidence measurements, a CFD. The bias voltage was between 1500 and 1800 volts to ensure single photon detection.

To reduce the background count rate the PMT was cooled to -30°C using an ethylene glycol cooling loop. A chiller unit was plumbed to flow coolant into pipes inside the vacuum chamber and into a large copper block that held the PMT. The room temperature dark count rate for the ET9426 was 500 cps, which dropped to 20 cps when cooled. The count rate was also elevated for a few hours after exposure to room light.

To verify the PMT was sensitive to individual photons, an energy spectrum was taken and compared to the single photon spectrum provided by the manufacturer. See Figure 3.8. The line in the figure at channel 36 shows approximately where the discriminator was set to minimize noise and maximize signal.

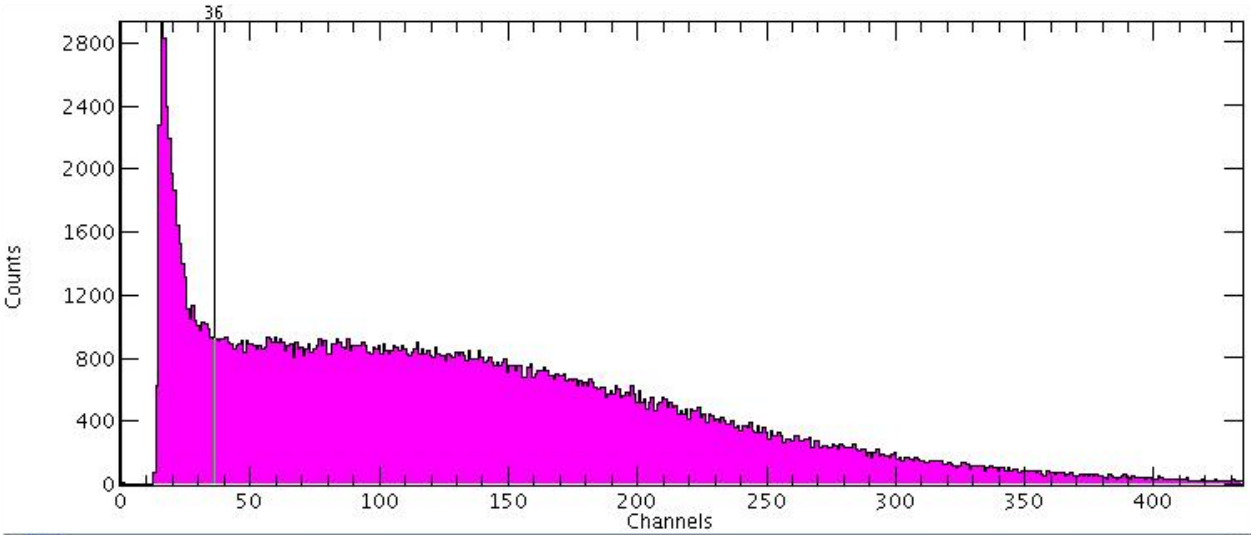

Figure 3.8: A pulse height spectrum taken from the ET9426 PMT with noise and 100 cps of signal from an LED. The peak at the low end is predominately noise, and the signal is predominately at higher energies. The line indicates the discriminator setting to maximize signal and minimize noise. The shape of the curve matches the curve supplied by the manufacturer indicating the PMT is detecting individual photons.

3.5 Methods of Measurements

3.5.1 Moving Catcher Method

Figure 3.9 shows the arrangement used to look for half lives from roughly 1 second to 2 days. The ^{233}U source (shown in Figure 3.4) is 2 inches in diameter and is located under the copper source shield. The catcher foils are 2.5 inches in diameter and are held by the catcher foil holder arms, which can be turned by a mechanism external to the vacuum chamber. The distance between the catcher and the source was approximately 2 mm. After the catcher had collected recoils for an appropriate amount of time it was moved over a detector, either an MCP or a PMT.

Electron detection uses an einzel lens to focus low energy electrons emerging from the catcher onto the MCP. SimION was used to model the einzel lens and MCP configuration. Figure 3.10 shows the results for electrons with a random initial energy between 1 and 7 eV and a randomly distributed initial direction. The front of the MCP is maintained at nominally +2000 V. The einzel lens consists of 5 electrodes maintained at potentials of 0, +1000, +4000, -4000, and +4000 volts, moving from the catcher towards the MCP. The MCP used in the moving catcher arrangement has an active area 25 mm in diameter. Based on SimION simulations the einzel lens focuses low energy electrons to a spot size of 13 mm. In addition to focusing the electrons, the einzel lens allows the MCP to be further from the catcher to reduce potential noise from daughter decays on the catcher.

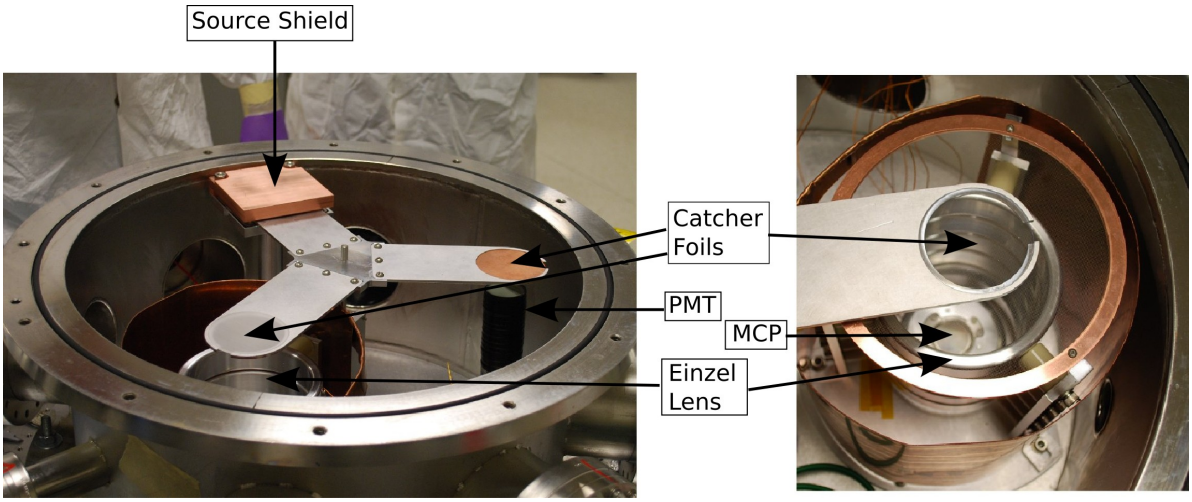

Figure 3.9: The moving catcher setup. On the left the three catcher foil holder arms are visible, as well as a PMT, the source holder, and the top of the einzel lens. On the right is a close up of the MCP system, including a transparent catcher foil, einzel lens, the MCP, the grid over the top of the MCP which reduces background electrons, and the copper shield which surrounds most of the einzel lens.

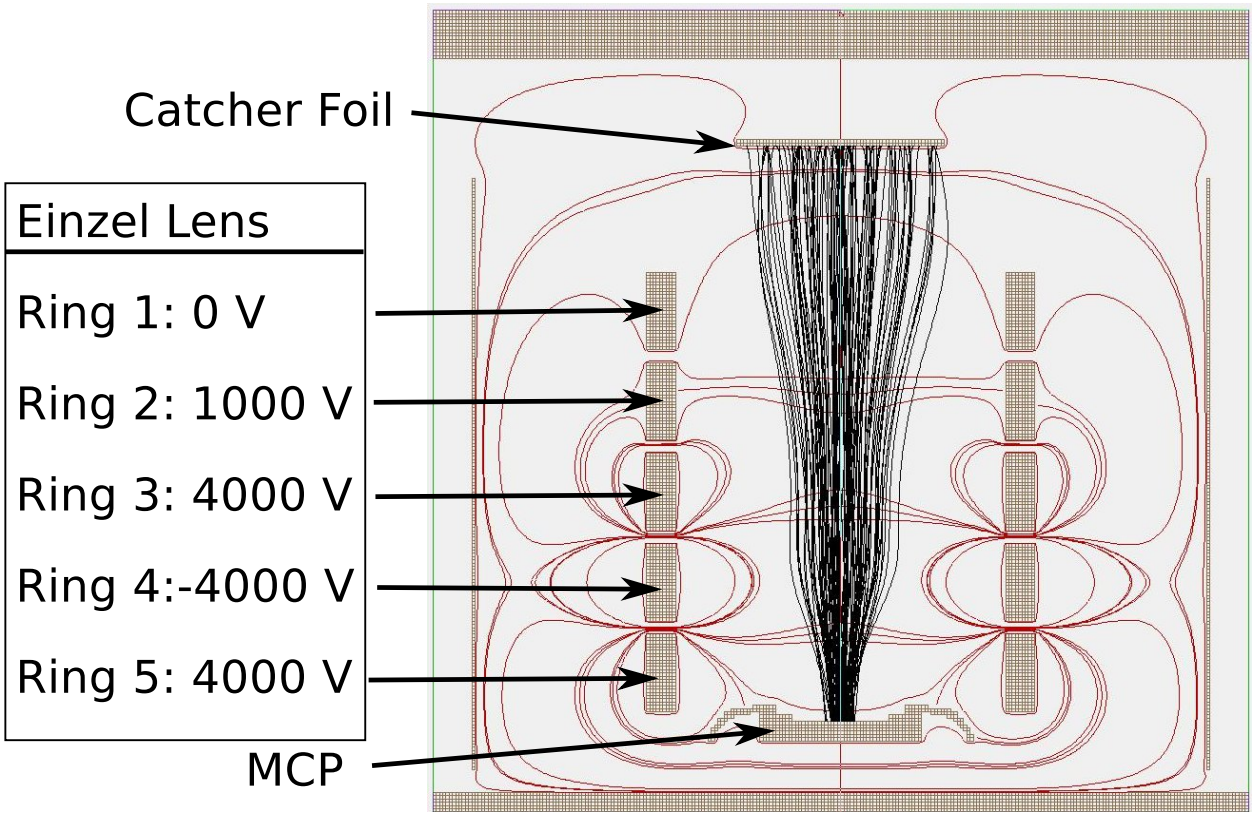

Figure 3.10: Cylindrically symmetric 2-dimensional einzel lens simulation in SimION. The catcher is located at the top, the MCP at the bottom, with the einzel lens on the sides. Red lines are equipotential lines, black lines are electron tracks. Electron energies were randomly distributed between 1 and 7 eV, with initial directions randomly distributed between 0 and 90 degrees from vertical. Einzel lens voltages are listed on the left side.

To reduce background counts, a fine mesh with 30 wires per inch and 95% open area was placed over the einzel lens assembly approximately 2 mm below the catcher. The mesh was typically maintained at -10 volts, and the catcher was maintained at -11 volts to ensure emitted electrons had enough energy to enter the accelerating area. The small negative voltage on the grid and catcher pushed background electrons away from the einzel lens and MCP and reduced background counts by a factor of ten or more. There was also a solid copper shield wrapped around the einzel lens assembly to prevent electrons from penetrating to the MCP. There is another copper shield over the source since it generates almost all the background electrons in the chamber. The efforts to reduce the MCP background yielded a background count rate of 10 counts per second (cps) with a source in the chamber. With no source in the chamber the background rate was about 1 cps, comparable to the rate of cosmic ray interactions with the detector.

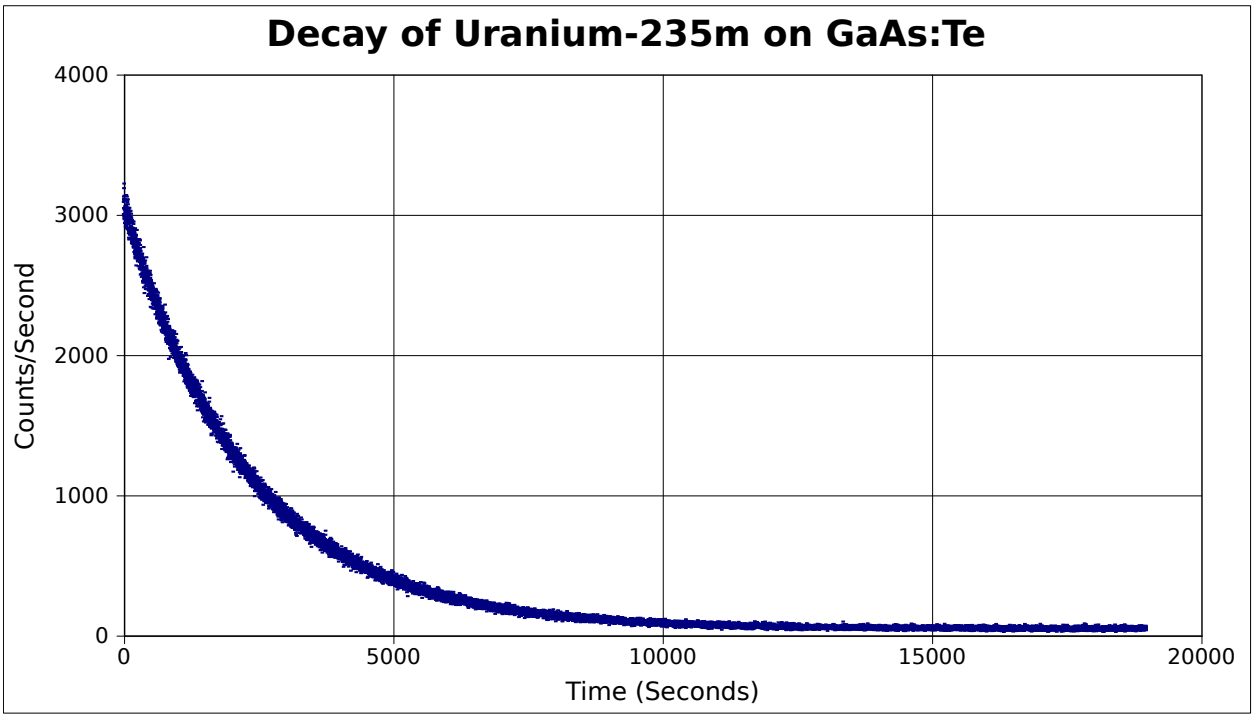

Figure 3.11: The decay of ^{235m}U measured on the MCP in the moving catcher arrangement. The catcher was GaAs:Te.

When using the PMT as a detector, the face of the PMT was in close proximity to the catcher, so no focusing was needed. The main source of background counts when using the PMT was the dark count rate of the PMT itself. Even after cooling, the background of the PMT was higher than the MCP, typically 20 cps.

This arrangement was sensitive to half lives from about 1 second to 2 days. The sensitivity decreases rapidly as half lives fall below a few seconds since 6 seconds pass while repositioning the catcher, allowing significant decay. Longer half lives are limited by the amount of time one is willing to spend collecting and measuring the decay. Long term variations in the background were also an issue. As an example, there were several occasions when the climate control systems in the laboratory were not functioning, and the temperature variations caused unacceptable changes in background count rates. It was also important to ensure the vacuum and the detector background had stabilized before starting a measurement.

A ^{239}Pu source was used to verify the proper functioning of the moving catcher arrangement. The ^{235m}U generated by the Pu has a 76 eV decay energy and a 26 minute half life, which was easy to see. Figure 3.11 shows a decay curve from ^{235m}U on GaAs:Te using the MCP. Table 3.2 lists the half lives measured for different catcher materials along with initial count rates. The different half lives are real changes in the half life brought about by the different conditions the ^{235m}U is in. This effect has been seen before[43][44][45]. These

measurements confirm the proper operation of the MCP and ART in the moving catcher measurement.

This arrangement was also run with the PMT to look for a decay curve from ^{235m}U via photons. No decay was observed. The decay of ^{235m}U is solely by IC. Even when using a scintillator (Eljen EJ-212) as the catcher, no decay was observed. The function of the PMT was confirmed with a pulsing LED instead.

3.5.2 Mechanical Shutter Method

To probe shorter time scales, a mechanical shutter was used with a one inch iris and an opening and closing time of 5 ms. Figure 3.12 shows the shutter opening and closing as measured by light passing through the iris. The shutter was used with both the MCP and the PMT. Figure 3.13 shows the mechanical shutter arrangement with the PMT. The source was placed on one side of the shutter and the catcher foil on the other. With the shutter open, recoiling Th atoms can reach the catcher from the source and build in. After the shutter closes, the isomer begins to decay away. Observing a decay would indicate the presence of the isomer. In theory, the build in could also be analyzed, but in reality the background from the source with the shutter open was far too large and caused significant dead time. Since the shutter iris was only 1 inch in diameter, only part of the 2 inch source was useful in this arrangement. This reduces the sensitivity compared to the moving catcher arrangement.

While using the MCP to detect electrons, various foils were tried including metals and semiconductors. The catcher was at an angle to the shutter, with the MCP close to the catcher. While the PMT was being used, only transparent catchers were used, and the PMT was located on the opposite side of the catcher from the shutter. Catchers tried

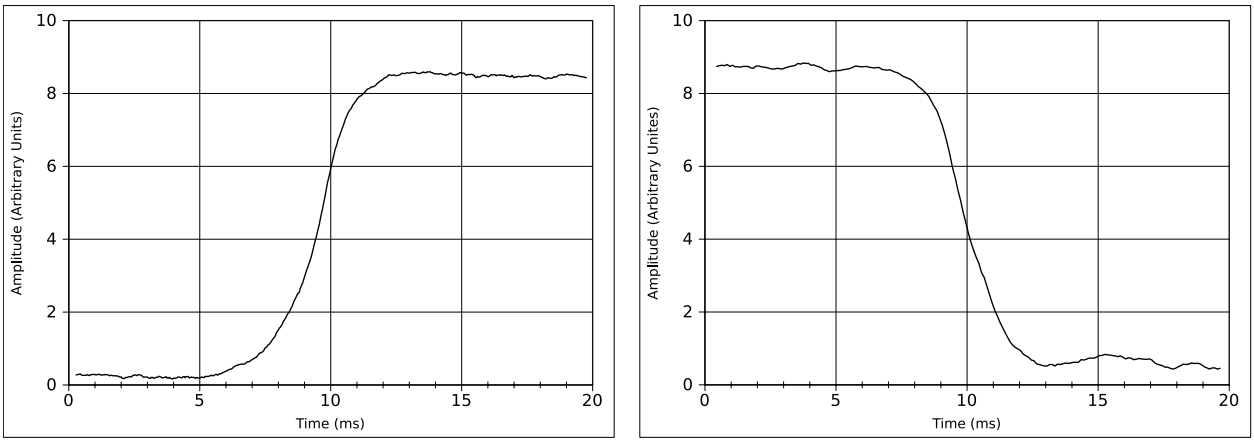

Figure 3.12: The mechanical shutter opening (left) and closing (right) as measured by a light sensitive silicon diode looking at a diffuse light source through the shutter.

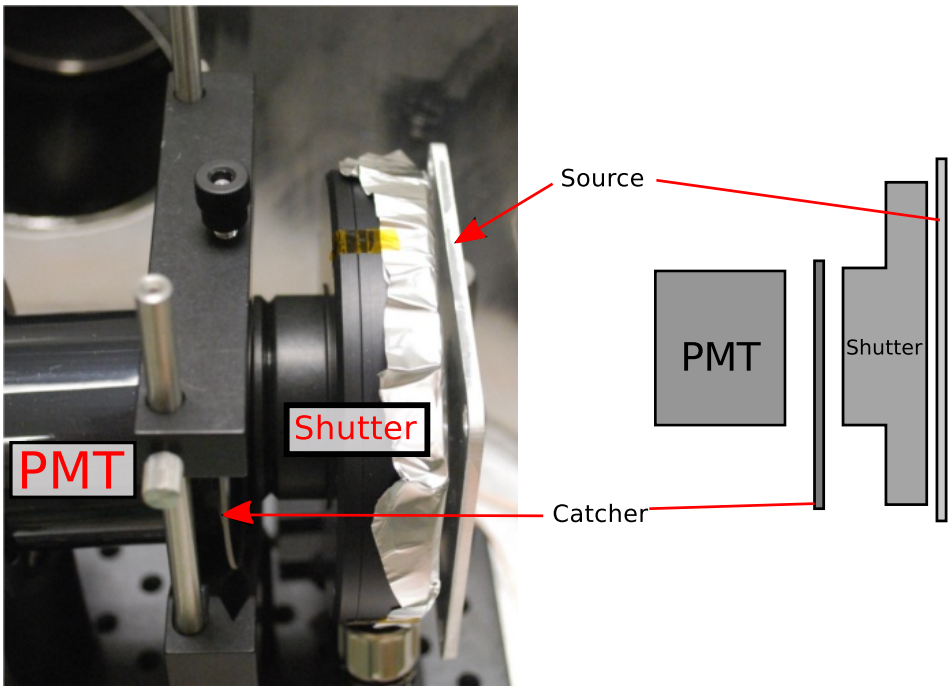

Figure 3.13: A picture (left) and diagram of the mechanical shutter arrangement while using the PMT. The catcher is transparent to light.

included MgF_2 and Al_2O_3. As noted before, these are both transparent over a wide range of wavelengths.

This particular technique was sensitive to half lives from 2 ms to 4.5 seconds (for the MCP) or 6 seconds (for the PMT). The short limit is determined primarily from the time it takes the shutter to close. The moving catcher arrangement was more sensitive to longer half lives, so the shutter was opened long enough to ensure overlap with the moving catcher measurements. The shutter was opened for 1 or 2 seconds and closed for 4 seconds. This was repeated thousands of times and the results summed. Events were recorded with a time stamp, and the closing time of the shutter was used as a reference. Sources of ^{234}U and ^{239}Pu were used for comparison and system validation.

Figure 3.14 shows the decay of ^{235m}U on GaN using the mechanical shutter. The ^{239}Pu source was 5.4 μCi. This clearly shows the mechanical shutter arrangement is less sensitive than the moving catcher foil. The shutter has the advantage of much faster measurements and the ability to repeat them numerous times.

An attempt to measure ^{235m}U with the PMT was also attempted with this setup, but again no signal was found. An LED was used to validate the proper functioning of the PMT.

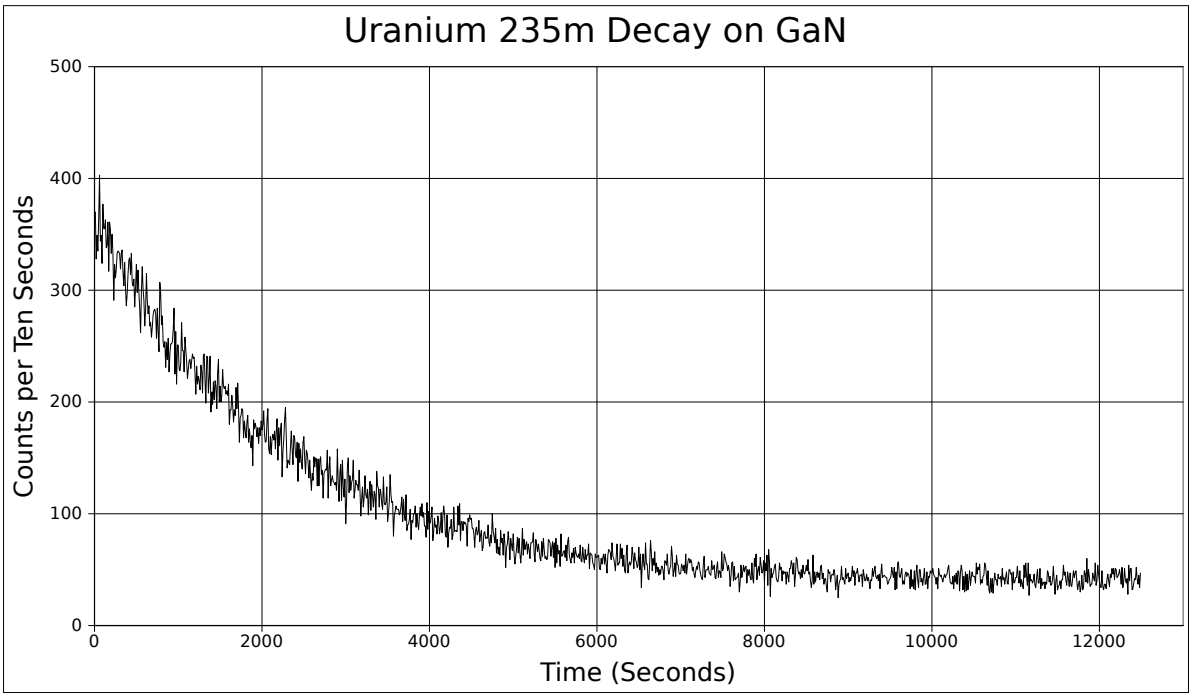

Figure 3.14: Measuring ^{235m}U for validation testing of the Mechanical Shutter.

3.5.3 Alpha Coincidence Method

Figure 3.15 shows the α-coincidence arrangement. This arrangement was sensitive to half lives as short as 40 ns and up to about 1 ms. The ^{233}U source used was 0.2 μCi deposited on a thin mylar backing. Recoiling nuclei can escape from the front of the source, although they cannot penetrate the mylar backing. The α particles can easily penetrate the mylar backing, loosing only 180 keV, allowing a coincidence measurement between the two. Since the α and recoiling nucleus move in opposite directions, the α detector and catcher were arranged such that an α detection should yield a recoil on the catcher. This ignores collisions, which rarely cause large changes of direction in a thin source on a thin substrate. Using the α particle as a start signal and the next signal on the MCP or PMT as a stop signal, a histogram of the times can be constructed to measure the half life of the isomer. The start and stop signals were fed to a Time to Amplitude Converter (TAC), and from there to an Analog to Digital Converter (ADC) which measured the amplitude.

At time scales this short, the time of flight (TOF) of recoiling nuclei are apparent. For example, an 84.4 keV ^{229}Th recoil takes 380 ns to travel 10 cm. The lighter α particles and electrons travel much faster. A 4 MeV α particle takes 7 ns to cover the same distance. A 10 keV electron covers the distance in less than 2 ns. The arrival of the recoiling atoms was clearly seen in the measurements. The timing agreed well with calculated arrival times. See Figure 3.16.

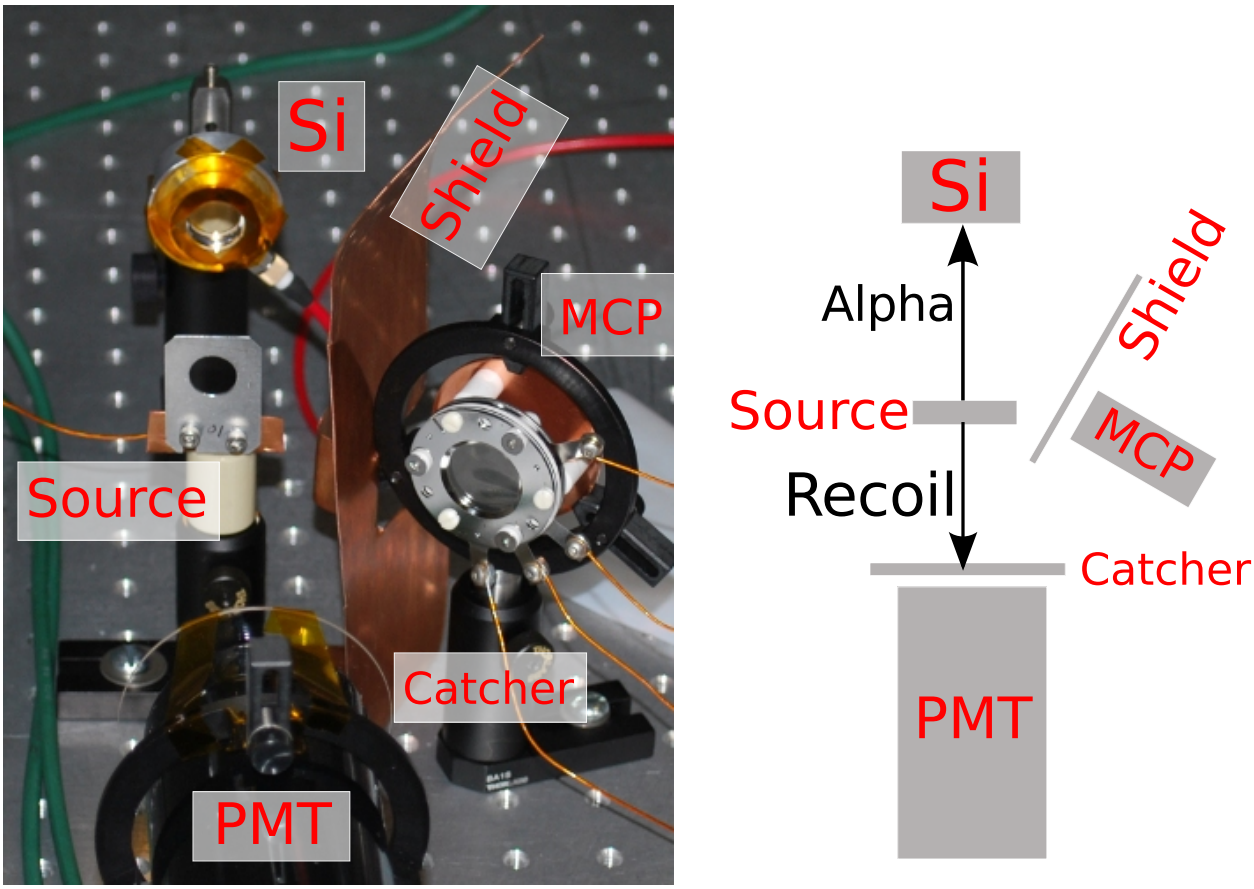

Figure 3.15: A picture and diagram of the alpha coincidence arrangement, including the PMT and MCP.

The detection of the recoils is an interfering signal. To avoid it, 2 different measurements were made. The simplest method started the TAC when the α was detected and stopped the TAC at the next signal from the MCP or PMT. A typical resulting spectrum is shown in Figure 3.16. The large peak at time zero results from either internal conversion electrons from the recoil or possibly electrons directly resulting from the α decay of the ^{233}U. The broader peak starting at about 400 ns is from the recoiling nuclei. With the source inserted backwards, the recoil peak disappears completely since the recoils cannot penetrate the mylar source backing. Measurements taken this way are only sensitive to very short half lives since the measurement has to stop before the recoils arrive. If not the measurement becomes very insensitive due to the large and varying background.

To avoid the recoil peak, another measurement measured the time between the α and the first MCP or PMT pulse that occurred more than a set time later, typically 600 ns. This allowed the recoils to be ignored while remaining sensitive to half lives longer than those

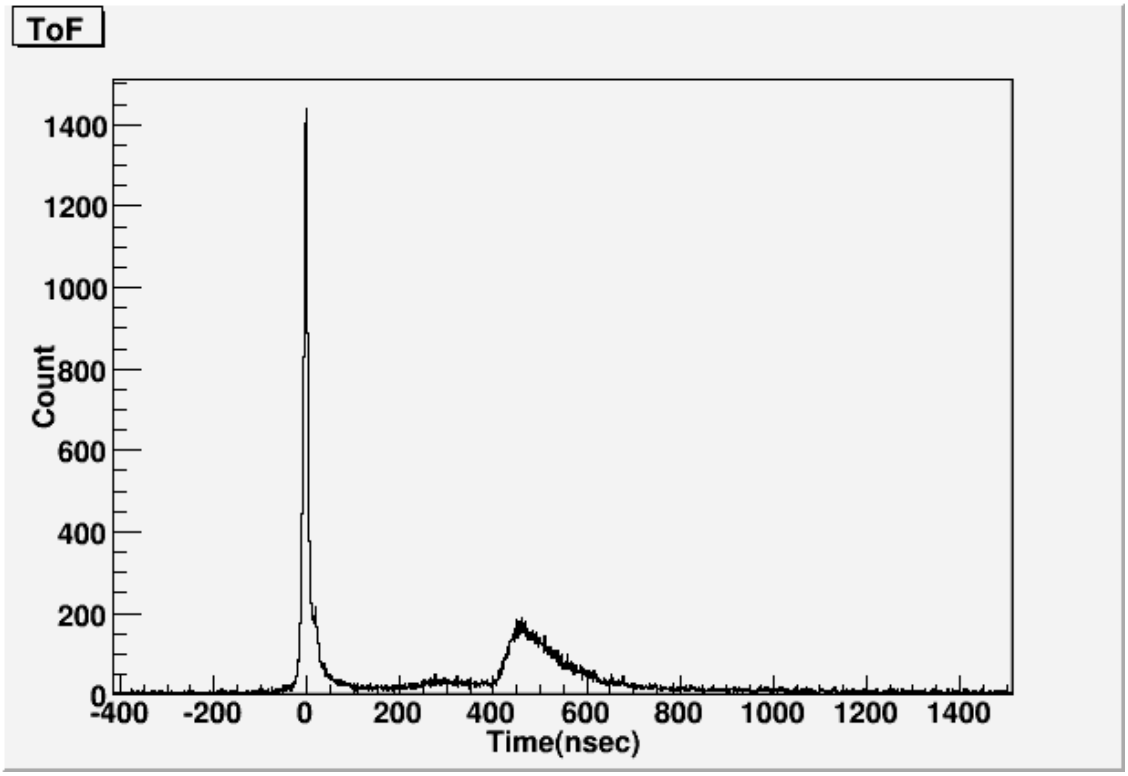

Figure 3.16: A plot of the Time of Flight (TOF) for the MCP using a Time to Amplitude Converter (TAC). The TAC start signal was from the Si α detector, and the stop signal was from the MCP. The MCP signal was delayed approximately 400 ns which allowed events before and after the α signal to be used. The first large peak, roughly in coincidence with the α signal, is from prompt events, perhaps internal conversion electrons. The next lower and longer peak is from recoiling nuclei.

measured without the delay.

In these measurements, the MCP itself was used as the catcher for electrons. This should increase the collection efficiency and reduce questions about the electrons escaping from the catcher. It was saved till last because the radioactive recoils will slowly build up on the MCP and start raising the background.

Metals					
Material	Electronegativity	Work Function (ev)	Band Gap (ev)	^{235m}U Half Life (seconds)	Count Rate (per second)
Al	1.61	4.06	0	1608.8±2.8	3035
Au	2.40	5.1	0	1605.5±1.9	4166
Cu	1.90	4.53	0	1597.0±0.9	3562
Y	1.22	3.1	0	1593.9±2.6	3000
Ti	1.54	4.33	0	1593.4±2.0	2354
In	1.78	4.09	0	1578.6±3.1	3724
Semiconductors					
Material	Electronegativity	Work Function (ev)	Band Gap (ev)	^{235m}U Half Life (seconds)	Count Rate (per second)
Si (I)	1.9	4.83	1.1	1614.5±2.3	1958
Si (P)	1.9		1.1	1613.7±4.0	2257
GaAs	2.0	4.71	1.43	1603.7±0.9	3096
Si (N)	1.9		1.1	1600.2±2.6	2791
Al_2O_3	2.71		8.8	1598.3±34	1560
GaP	2.0		2.26	1598.0±1.8	3510
Ge	2.01	4.8	0.67	1597.5±2.5	3000
SiO_2	2.93		8.4	1594.1±3.5	556
GaN	2.43		3.4	1538.5±10	870

Table 3.2: The catcher materials used and some of their properties. Metals are listed first, followed by semiconductors. For compounds the electronegativity is simply a weighted average of the elements. The work function of a material depends on many things, including the crystal orientation of the surface and surface impurities. The work functions listed here are representative. Notice that the measured half life for ^{235m}U changes depending on the catcher material, as does the initial count rate. The electronegativity values are from [48], the work functions for metals are from [49], other work functions are from [50], band gaps are from [51] except for Al_2O_3 and SiO_2 which are from [52].

Chapter 4

Results

Three different types of measurement were made, each searching for electrons and photons. Although the decay of the isomer was not found, exclusion plots were made to show what conditions the present experiments were sensitive to. Hopefully these will prove useful to future researchers.

This chapter starts with a description of the analysis methodology used to determine if the isomer was seen. They are applicable to each of the measurement techniques used with minor adjustments. Then the results of each of the techniques is described in turn. Lastly the results are combined to yield exclusion plots for the MCP and the PMT.

4.1 Analysis Methodology

Tests to determine if a signal is present are generally more sensitive than measurements of a half life. Therefore the first step in the data analysis was to look for a signal indicating the presence of a decay from ^{229m}Th. Since no signal was detected, detection limits were calculated to determine what signal would have been seen. The detection limits are then converted from counts to exclusion plots.

The method used to determine if a signal is present, and the associated detection limit if not, is based on the work of Currie[53]. Normally a separate background measurement is performed and compared to the actual measurement. In these experiments, the background level is sensitive to the exact details, such as the position of the catcher foil over the detector, so a separate background measurement was not used. Instead a longer measurement was made and the end of the measurement was used as the background. When computing the minimum detectable activity, the possible effect of a long half life decay not reaching background was included.

See Figure 4.1 for nomenclature. Two regions of the measurement are used, called the signal region and the background region. Time t=0 is when the catcher stops collecting recoils. The signal region does not start at t=0. This is because of the time it takes to

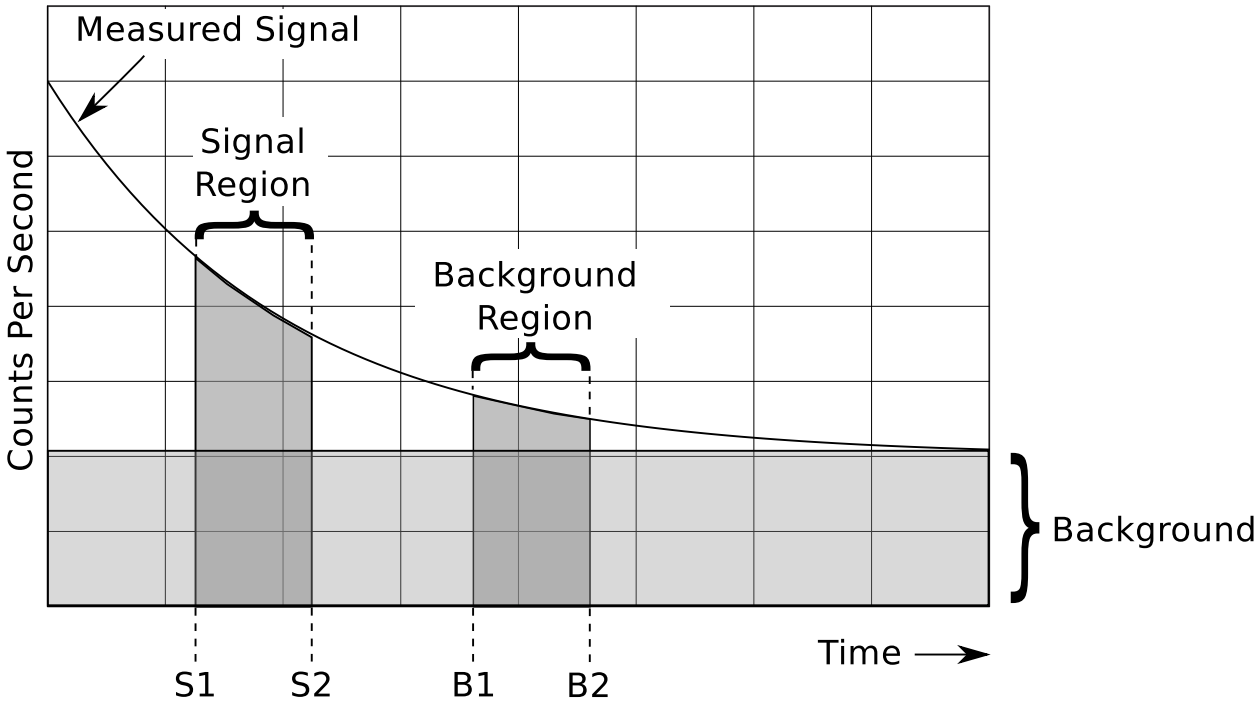

Figure 4.1: An idealized signal, with a greatly exaggerated decay and perfect statistics. The signal region is the part of the data being used to determine if any signal is present above background. It starts at S_1 and ends at S_2, both in seconds. The background region is used to estimate the background level. It starts at B_1 and ends at B_2. For relatively long half lives, some of the signal can be present in the background region. This was accounted for in determining the detection limit, L_D.

physically move the catcher in the moving catcher technique, the time required for the shutter to close in the mechanical shutter technique, and the time required for signals to travel the wire in the alpha-coincidence technique.

The length of both regions was varied, independently without overlapping, to maximize the sensitivity for various half lives. The algorithm started with the signal region only three channels wide, and the background region started one channel past the signal region. The results, calculated using the method described next, were saved for a range of half lives, and then the start of the background region was moved forward in time, the background region thus becoming smaller. The background was repeatedly shrunk, saving the best results independently for the various half lives at each size, until the background region was a minimum size, typically 100 channels wide. Background regions smaller than this typically yield worse results. Then the size of the signal region was increased, and the background region varied again. The entire process was repeated until the signal region left only enough space for the minimum background region size. This process finds the best signal and

background regions for a range of half lives, in preparation for generating an exclusion plot.

The results referenced above are termed the Minimum Detectable Initial Count Rate (MDICR). The MDICR is the minimum count rate at time t=0 that, statistically speaking, would have been detected. There are several steps to the calculation. First, the means for both regions are calculated

$$\mu_{\mathrm{S}} = \frac{1}{\mathrm{S_2} - \mathrm{S_1}} \sum_{\mathrm{i=S_1}}^{\mathrm{S_2}} \mathrm{x_i} \quad \text{and} \quad \mu_{\mathrm{B}} = \frac{1}{\mathrm{B_2} - \mathrm{B_1}} \sum_{\mathrm{i=B_1}}^{\mathrm{B_2}} \mathrm{x_i} \tag{4.1}$$

The signal mean is μ_{S}, the background mean is μ_{B}, and $\mathrm{x_i}$ are the counts in individual channels. $\mathrm{S_1}$, $\mathrm{S_2}$, $\mathrm{B_1}$, and $\mathrm{B_2}$ are as above. The difference in the means, $\mu_{\mathrm{S}} - \mu_{\mathrm{B}}$, is compared to the critical level (defined next) to determine if a signal is present or not.

The critical level, or $\mathrm{L_C}$, is the difference of the means above which a signal is said to be present. $\mathrm{L_C}$ is determined from

$$\mathrm{L_C} = \mathrm{k}_\alpha \sigma_0 \tag{4.2}$$

where k_α is a multiplier used to determine the confidence level and σ_0 is the standard deviation. The value of k_α used here is 1.645, which corresponds to a 5% false positive rate or 95% confidence that a measurement above L_C is a real detection. The standard deviation is for the measurement. In this case the measurement is the difference of the means of the two regions, and the standard deviation for their difference is just their individual standard deviations added in quadrature

$$\sigma_0 = \sqrt{\sigma_{\mathrm{S}}^2 + \sigma_{\mathrm{B}}^2} \tag{4.3}$$

The sample standard deviation was used for the regions, computed using the usual formula

$$\sigma = \sqrt{\frac{\sum_{\mathrm{i=1}}^{\mathrm{N}} (\mathrm{x_i} - \mu)^2}{\mathrm{N} - 1}} \tag{4.4}$$

For a normal or Poisson distribution the standard deviation is the square root of the mean divided by the square root of the number of measurements. The sample standard deviations calculated using Equation 4.4 were larger than expected for a Poisson distribution by typically 10-20%. This larger value was used in computing $\mathrm{L_C}$.

The next step is to determine the detection limit, or $\mathrm{L_D}$. This is the number of counts from a true signal that would have been reliably detected, taking into account the statistical nature of the background. L_D is defined as

$$\mathrm{L_D} = \mathrm{L_C} + \mathrm{k}_\beta \sigma_0 \tag{4.5}$$

where k_β serves the same purpose as k_α except it weights for false negatives now. The standard deviation σ_0 in principle can be different from that used to find $\mathrm{L_C}$, but in the present experiment they are the same. If $\mathrm{k}_\beta = \mathrm{k}_\alpha$ then $\mathrm{L_D}$ is simply twice $\mathrm{L_C}$. This value,

$L_D = 2L_C = 3.29\sigma_0$, is used in this experiment. These values of L_C and L_D yield a false positive rate (concluding a signal is present when none is) and a false negative rate (concluding a signal is not present when it actually is) of 5%.

Two corrections, due to half lives, are needed to convert from L_D to MDICR. Since these are half life specific, each half life has a corresponding MDICR. Here, half life refers to a hypothetical half life, the decay of which we're searching for. The first correction accounts for how the signal decays from time t=0. It is

$$\frac{\lambda}{\frac{e^{-\lambda S_1}-e^{-\lambda S_2}}{S_2-S_1} - \frac{e^{-\lambda B_1}-e^{-\lambda B_2}}{B_2-B_1}} \tag{4.6}$$

There are three primary effects from this correction. Firstly, very short lived decays might not contribute any signal to the signal region due to the delay between t=0 and S_1. Secondly, moderately long decays will be decaying during the signal region and contribute fewer counts than if they were longer lived. Lastly, long decays will contribute signals to the background region as well as the signal region, reducing sensitivity. This correction accounts for all three.

The second correction is for the collection time. During collection, the decay of the isomer on the catcher will approach an equilibrium value. While the equilibrium value is fixed, a longer half life decay takes longer to reach it. This term, strictly speaking, does not belong in the MDICR since it does not change the minimum count rate needed for detection. It is included here because then all terms affected by half life are collected within the MDICR. This makes future calculations easier. This correction factor is simply

$$\frac{1}{1-e^{-\lambda t}} \tag{4.7}$$

Combining the above yields the MDICR

$$\mathrm{MDICR} = \frac{L_D}{(1-e^{-\lambda t})} \cdot \frac{\lambda}{\frac{e^{-\lambda S_1}-e^{-\lambda S_2}}{S_2-S_1} - \frac{e^{-\lambda B_1}-e^{-\lambda B_2}}{B_2-B_1}} \tag{4.8}$$

Still remaining to be incorporated are the efficiency of the detectors (η_{det}), the source activities ($A(^{233}U)$), the branching ratio from the α decay of ^{233}U to the isomer (BR_{iso}), and the branching ratio from the isomer to either internal conversion (BR_{IC}) or γ decay (BR_γ). The first two will vary by the measurement technique. BR_{iso} will be set to 2.6%, which is the sum of the 2.1% indirect branching ratio estimate from Barci[11] and the direct branching ratio from ^{233}U α decay as estimated in Chapter 2. BR_{IC} (for electron measurements) or BR_γ (for photons) will be an axis on the exclusion plots. They are incorporated as follows.

To begin, the maximum signal that could be seen, A_0, can be found assuming that the source and the catcher had reached equilibrium before the catcher was moved. If equilibrium has not been reached, this has already been incorporated into the MDICR results. Both branching ratios can also be incorporated at this step. BR with no subscript represents

either IC or γ decay, as appropriate to the measurement. At equilibrium the recoiling isomers will decay as fast as they are collected from the source, or

$$A_0 = A(^{233}U) \cdot \eta_{recoil} \cdot BR_{iso} \cdot BR \tag{4.9}$$

Once the initial activity has been found, it can be converted to an expected Initial Count Rate (ICR) based on the detector efficiency η_{det}

$$ICR = A_0 \cdot \eta_{det} \tag{4.10}$$

The efficiencies will be different for the MCP and the PMT, and also for the different experiments. In total the initial count rate is

$$ICR = A(^{233}U) \cdot \eta_{recoil} \cdot BR_{iso} \cdot BR \cdot \eta_{det} \tag{4.11}$$

The source activity is known and the recoil efficiency has been measured or estimated. We can estimate the electron detection efficiency from ^{235m}U measurements, with the caveat that there is no guarantee the electrons will have enough energy to escape. The PMT quantum efficiency and the geometric efficiency can be used to estimate the detection efficiency for the PMT. Then we can generate an exclusion plot by setting ICR equal to the MDICR and solving for the appropriate branching ratio. The exclusion plots show BR_{IC} or BR_γ above which a true signal should have been detected for the various half lives.

4.2 Moving Catcher Results

The moving catcher setup was used to search for half lives from approximately one second to a few days. The sensitivity of these measurements decreases as the half life decreases due to the time required to reposition the moving catcher (6 seconds), which would allow a short lived isomer to decay away. The sensitivity decreases as the half life increases due to the greater amount of signal present in the background region and the limited collection time of the isomer on the catcher foil. It is unlikely that the half life of the isomer is longer than several hours due to both theoretical calculations and to limits from previous experiments. The MCP results will be discussed first, followed by the PMT results.

A number of materials were used as catchers during electron measurements. These are listed in Table 3.2. Yttrium was the lowest work function material used, and it was shipped and handled in an argon atmosphere to prevent or at least limit oxidation. Several semiconductors were also used, with GaAs:Te having the best combination of high electron yield and the most reproducible half life for ^{235m}U. The reproducible half life is important as it indicates there are fewer exoelectrons or other sources of noise contributing to the measured signal. Several metals were tried, all with similar results. Copper was chosen as representative. The other materials yielded similar results but with higher detection limits. Typical data for GaAs:Te, copper, and yttrium is shown in Figure 4.2.

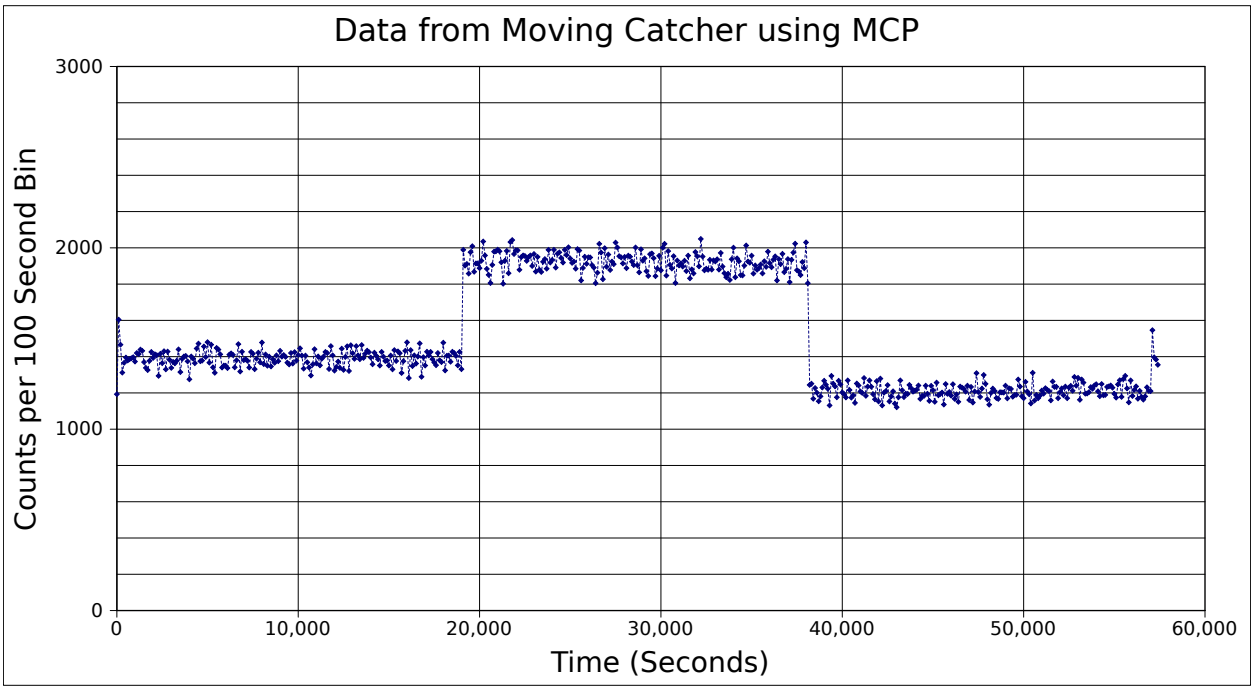

Figure 4.2: Typical data from the moving catcher experiment using the MCP. Note that the data has been put into 100 second bins for clarity, although the actual data was taken in 1 second bins. Three regions are clearly visible, corresponding, from left to right, to a measurement of the GaAs:Te, the copper, and the yttrium catchers. Spikes can be seen in the count rate while the catcher was rotating from one catcher to the next. Each measurement was 19,000 seconds long.

BR_{IC} versus half life for Y, Cu, and GaAs:Te on the MCP are plotted in Figure 4.3. The measurement times and collection times were all 19,000 seconds. The source used was ^{233}U with an activity of 3.29 μCi. The measured recoil collection efficiency was 38%. From ^{235m}U measurements η_{e^-} was about 2%, but this number varied from 0.28% in quartz to 7.2% in sapphire with a high electric field across it (the electric field caused instabilities which made it unusable). Since ^{229m}Th was never detected the actual efficiency is unknown, and will likely vary depending on catcher material. An efficiency of 2% was used, along with the other numbers above, to generate the exclusion plot of Figure 4.3. While there is no particular justification for using 2%, it is on the lower end of ^{235m}U η_{e^-} (2% corresponds to an initial count rate of 3,000 cps in Table 3.2), and some reasonable number is needed to generate the plots. As mentioned previously, there is no guarantee that electrons can escape from the catcher at all.

The moving catcher setup with the MCP was run at different speeds. Since the three catcher foils are moved together, the times for collecting the recoiling nuclei, counting the

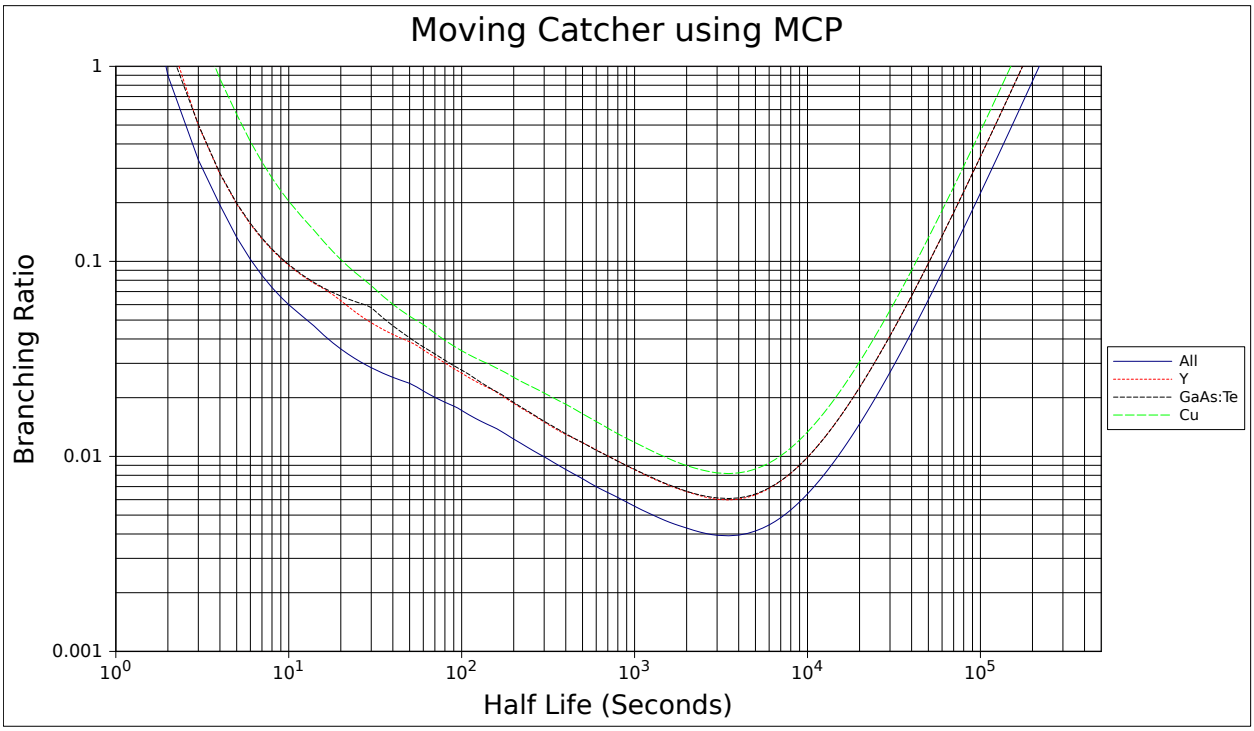

Figure 4.3: The minimum detectable internal conversion branching ratio determined for Y, Cu, and GaAs:Te. The lowest result is for the sum of the measurements of the three catchers.

recoiling nuclei, and waiting in between, are the same. Figure 4.4 shows the results for times of 5 minutes, 30 minutes, and 5 hours with results from Y, Cu, and GaAs:Te experiments summed. The shorter measurements are obviously less sensitive at longer half lives. At shorter half lives the only difference is in the number of times the experiment was repeated. In Figure 4.4 the 30 minute experiment was run more times than the 5 minute experiment, and so the 5 minute experiment never had a lower detection limit than the 30 minute measurements.

Data for the PMT measuring the acrylic catcher is shown in Figure 4.5. The results for the PMT measurements are shown in Figure 4.6. The values for the source activity and recoil collection efficiency are the same as for the MCP. The collection time for these measurements was 64,800 seconds. The detection efficiency can only be estimated. Using conservative values, the quantum efficiency of the PMT was more than 10% for most of it's spectral range, so we'll use 10%. The catchers were within a few mm of the PMT and had the same area, so we'll estimate the geometric efficiency as 40%, for a total detection efficiency of 4%. These are the values that were used in the exclusion plot of Figure 4.6. EJ-212 is a plastic scintillator that was used in the hope that conversion electrons would generate a scintillation signal. No such signal was seen with ^{229m}Th or ^{235m}U. The acrylic

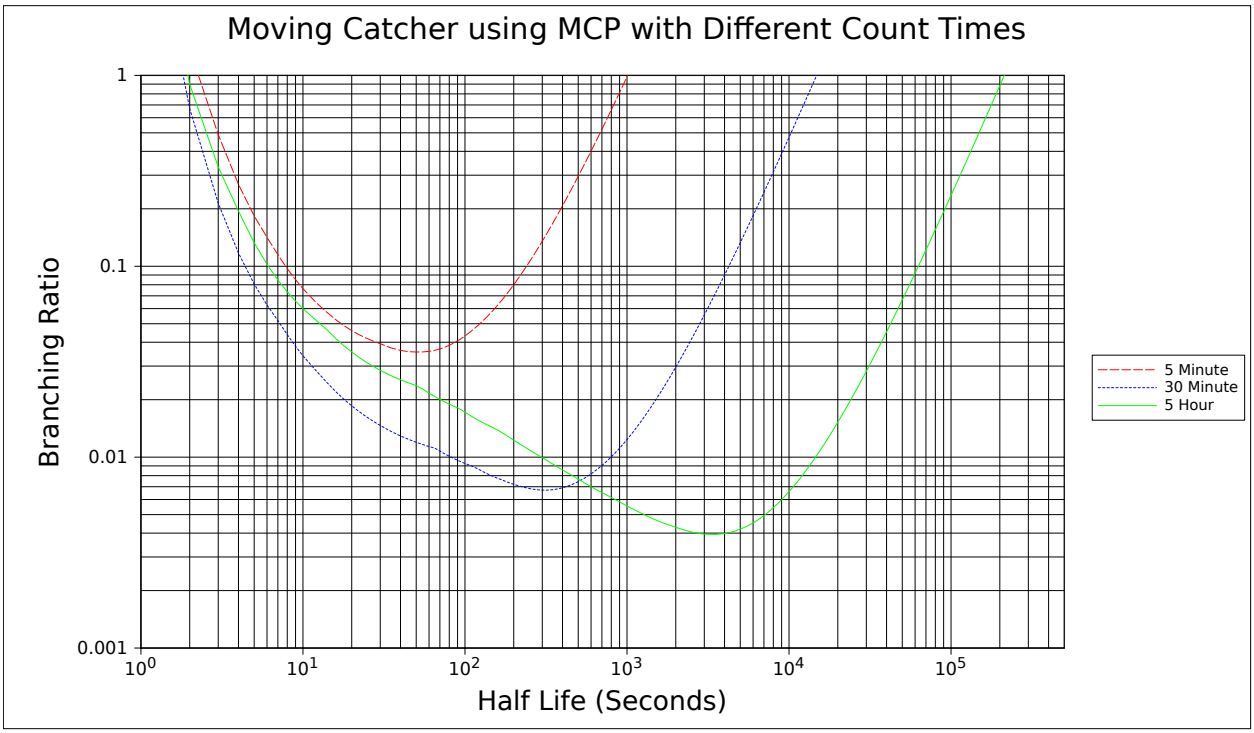

Figure 4.4: The minimum detectable internal conversion branching ratio determined for measurements of 5 minutes, 30 minutes, and 5 hours. The sensitivity at shorter half lives is increased primarily due to a larger number of measurements being conducted. Since a similar number of 5 minute measurements and 30 minute measurements were conducted, there was no increase in sensitivity. At longer half lives the shorter measurements are less sensitive due to both the shorter measurement length and the shorter collection time.

was a non-crystalline transparent material that was on hand. Titanium is not transparent, but the recoils were collected on the same side of the catcher that was exposed to the PMT. The recoils also embed very shallow in the catcher, which should allow photons to escape.

As with the MCP, other materials were measured with the PMT. The results from other metals were similar to titanium. Some materials, notably MgF_2 and, to a lesser extent, Al_2O_3, exhibited an afterglow that was undesirable. The afterglow was the same with a ^{233}U and ^{239}Pu source and was either non-exponential or had several exponential components. The materials with an afterglow were not used.

4.3 Mechanical Shutter Results

The analysis of the mechanical shutter data is very similar to that for the moving catcher arrangement. The biggest difference is the number of times the measurements were repeated,

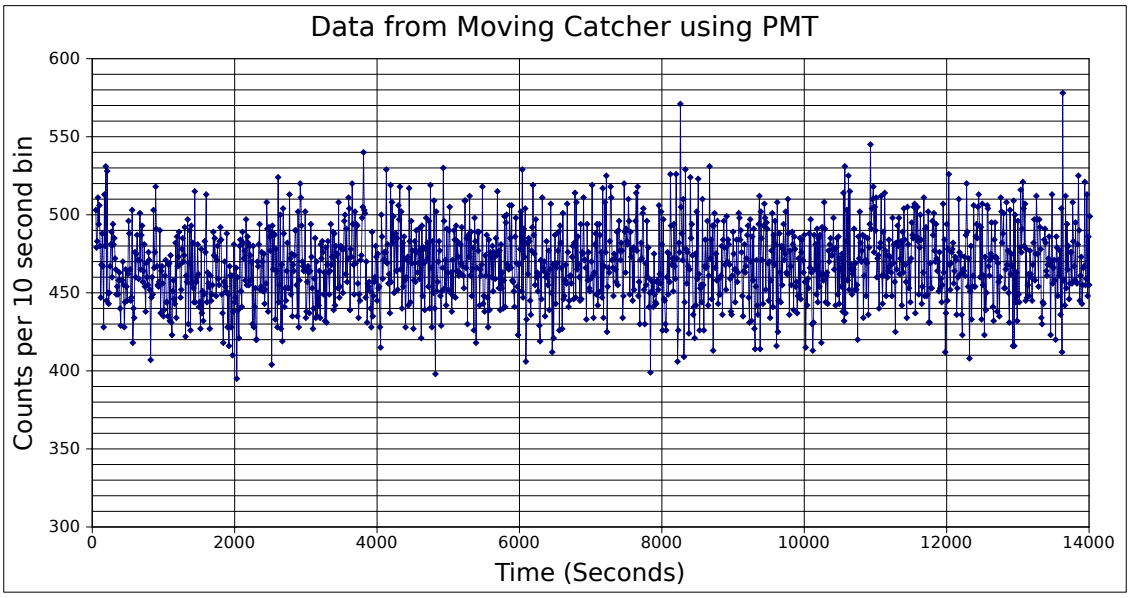

Figure 4.5: Typical data from the moving catcher experiment using the PMT. The data is in 10 second bins. This measurement was of the acrylic catcher foil.

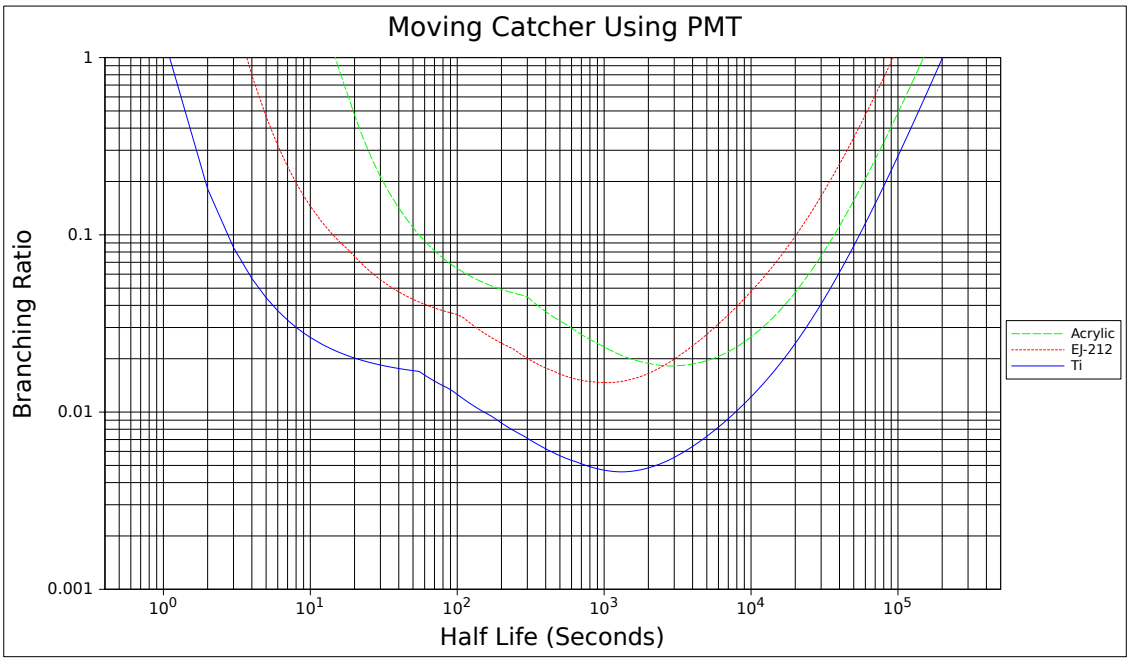

Figure 4.6: The minimum detectable γ branching ratio for the moving catcher arrangement using the PMT with acrylic, titanium, and EJ-212 catchers.

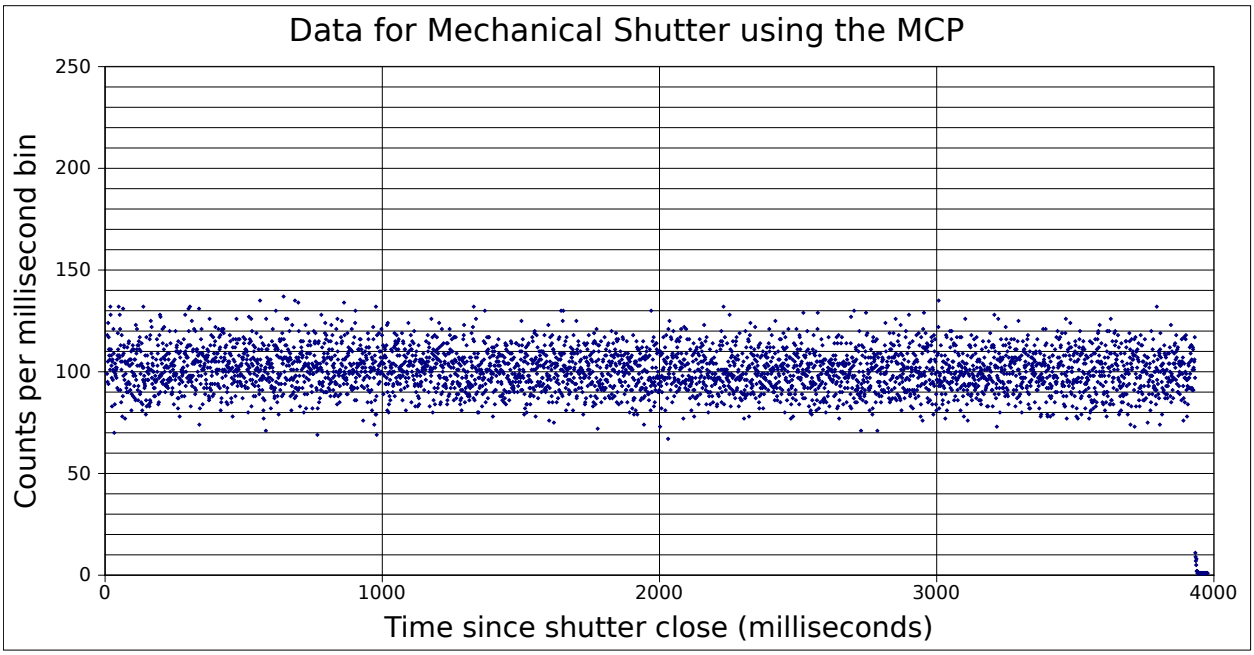

Figure 4.7: This is the data used for the mechanical shutter using the MCP. The catcher was GaN. The data are in 1 ms bins. All 12,795 shutter cycles were added together for this figure. Time = 0 is 7 ms after the shutter began closing.

which was many thousands instead of just a few. Unfortunately the shutter broke before the experiment was finished, but not before useful data was collected. It did limit the number of catcher foils that were measured.

The mechanical shutter technique is not as efficient as the moving catcher technique in terms of recoil collection and electron detection, but this is partially offset by the ability to make a large number of measurements. No recoil collection efficiency measurement was attempted with the shutter because the collection and counting times would have been prohibitively long. The recoil collection efficiency and electron collection efficiency can be estimated using the initial count rate and the source activity for ^{235m}U. Figure 3.14 shows the decay of ^{235m}U in the mechanical shutter arrangement. The source strength was 5.38 μCi. But the source was evenly distributed over a 2 inch circle, and the shutter was 1 inch wide. This means only 1/4 the source area was used, so the effective source strength was only 1.35 μCi. From this source, SRIM estimates 43% of the recoiling ^{235m}U will escape the source. The shutter also has a thickness of almost 1 inch, which further reduces the number of recoils that will reach the catcher by a factor of 1/4, the other recoils hitting the inside of the shutter walls. Of the 200,000 recoils per second generated by the entire 2 inch source, only 5370 will reach the catcher, or about 2.7%. With an initial count rate of 32 counts per second, the electron detection efficiency is 0.6%, which is very similar to the GaN electron

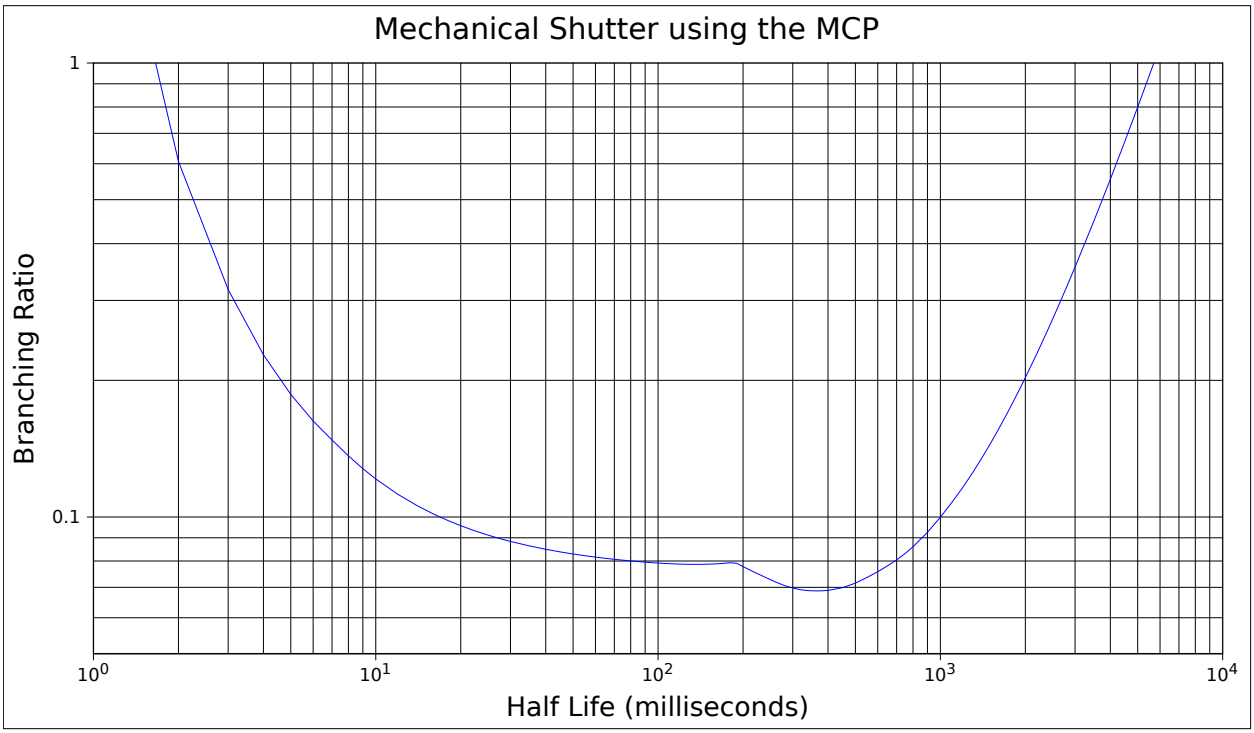

Figure 4.8: The minimum detectable internal conversion branching ratio for the mechanical shutter arrangement using the MCP and a GaN catcher.

efficiency of 0.58% with the moving catcher arrangement.

With the MCP, the shutter was cycled 12,795 times, with 1 second open followed by 4 seconds closed. A GaN catcher was used. The ^{233}U source, the same as used for the moving catcher, is 3.29 μCi and the measured recoil escape fraction is 38%. As above, only 1/4 of the source is used, and only 1/4 of the escaping recoils make it to the catcher. This leaves 2890 recoils per second arriving at the catcher. This will be the same for the PMT measurements as well. The electron efficiency is 0.6%, as above. The data is shown in Figure 4.7. The results are in Figure 4.8.

The PMT was used with the mechanical shutter as shown in Figure 3.13. Since light has to traverse the catcher in this arrangement, the catcher materials must be transparent in the region where the ^{229m}Th γ would occur. Two materials were tried as catchers, MgF_2 and sapphire (Al_2O_3). These were the only two readily available materials that are transparent to the potential gamma ray from the isomer. MgF_2 proved unusable due to it's very large fluorescence, as seen in Figure 4.9. A thin layer of plastic (1.5 mg/cm^2) was between the source and the shutter during that measurement, so recoils could not reach the catcher. Thus the glow is from the MgF_2 and not ^{229m}Th.

The PMT measurement was carried out using sapphire. The data is shown in Figure 4.10.

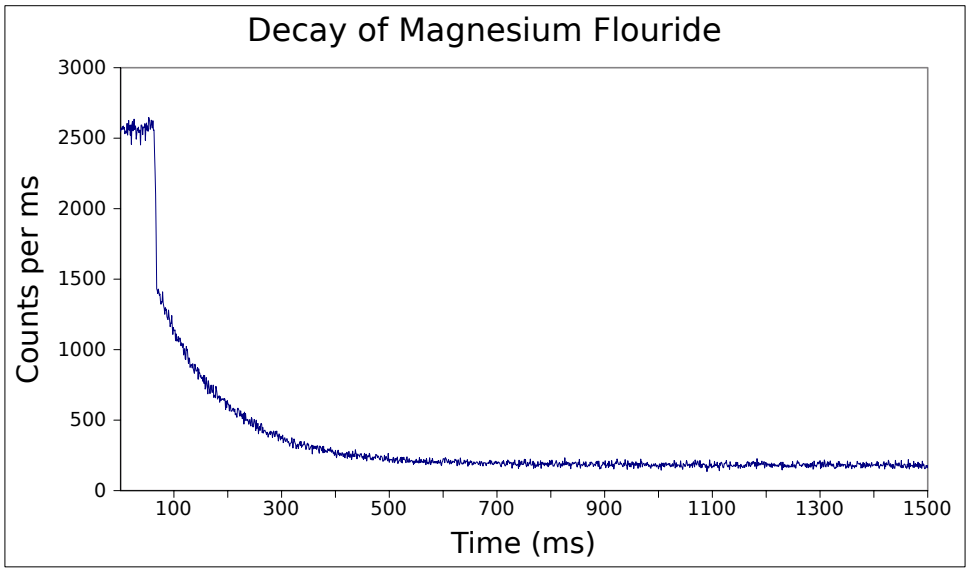

Figure 4.9: This plot shows the decay of the afterglow of MgF_2 after exposure to the ^{233}U source through a thin sheet of plastic. The plastic prevents the recoil nuclei from reaching the catcher, showing the afterglow is due to the MgF_2 glowing after exposure to α and β particles from the source. The shutter closed at the almost vertical line in the data near 80 ms.

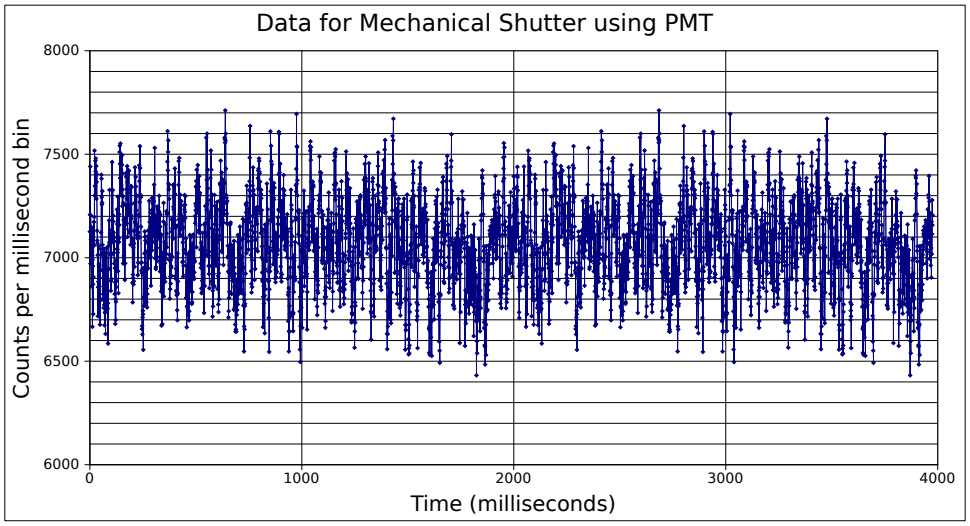

Figure 4.10: This is the data used for the mechanical shutter using the PMT. The catcher was sapphire. The data are in 1 ms bins. All 51,548 shutter cycles were added together for this figure. Time = 0 is 7 ms after the shutter began closing.

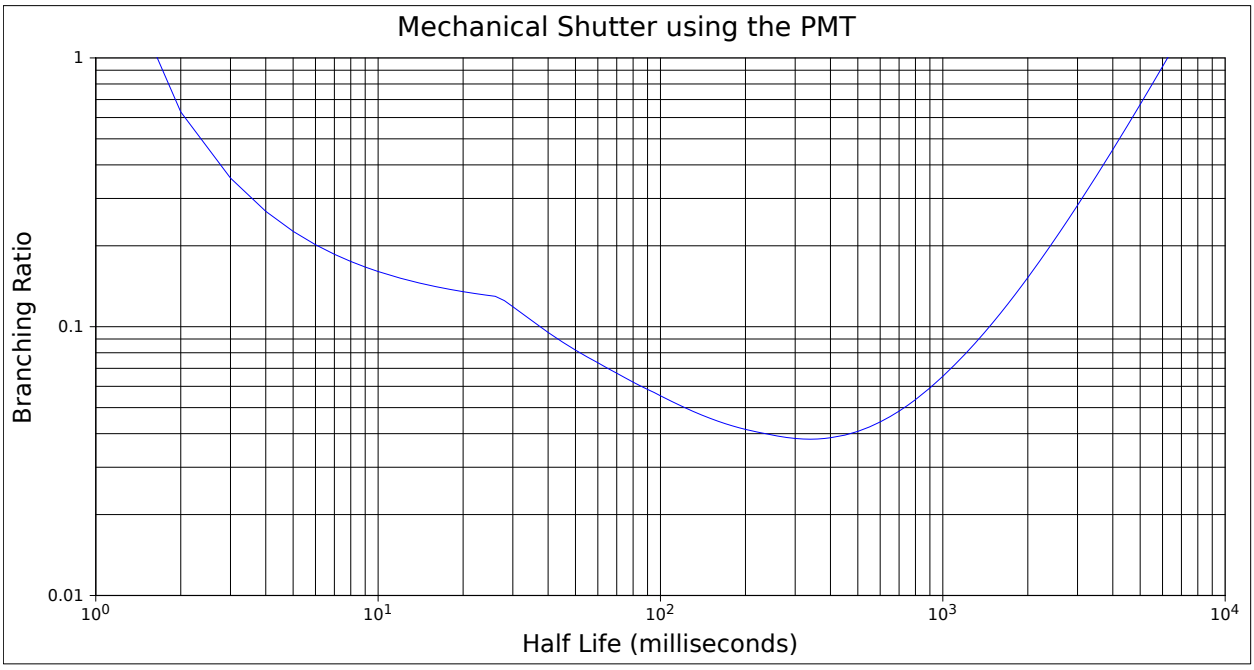

Figure 4.11: The minimum detectable photon branching ratio for the mechanical shutter arrangement using the PMT and a sapphire catcher.

The shutter cycled 51,548 times, opening for 2 seconds and closing for 4 seconds. The quantum efficiency was again assumed to be 10%, and the geometric efficiency 40%. As above, 2890 recoils arrive at the catcher per second. The results are shown in Figure 4.11.

4.4 Alpha Coincidence Results

The analysis for the alpha coincidence is slightly different than the others. In the previous experiments, a number of recoils N was collected over a period of time and then counted. N was never calculated directly but rather the activity was calculated based on the activity of the source, the length of the collection time, the branching ratio, and η_{recoil}. With the alpha coincidence measurements a count is made each time a recoil is captured, as indicated by detecting an alpha particle. There is no collection of N recoils that is counted for decays as a group. Instead N is measured directly, and the activity is calculated based on an assumed λ, which is varied.

The MDICR is still calculated and used as the minimum signal needed. But now the activity is calculated and depends on the λ used. This changes the calculations in a few ways. The first is that the factor $(1 - e^{-\lambda t})$ is assumed to be one because the recoil is collected and counted individually, and there is no need for the activity to build up. The initial count rate

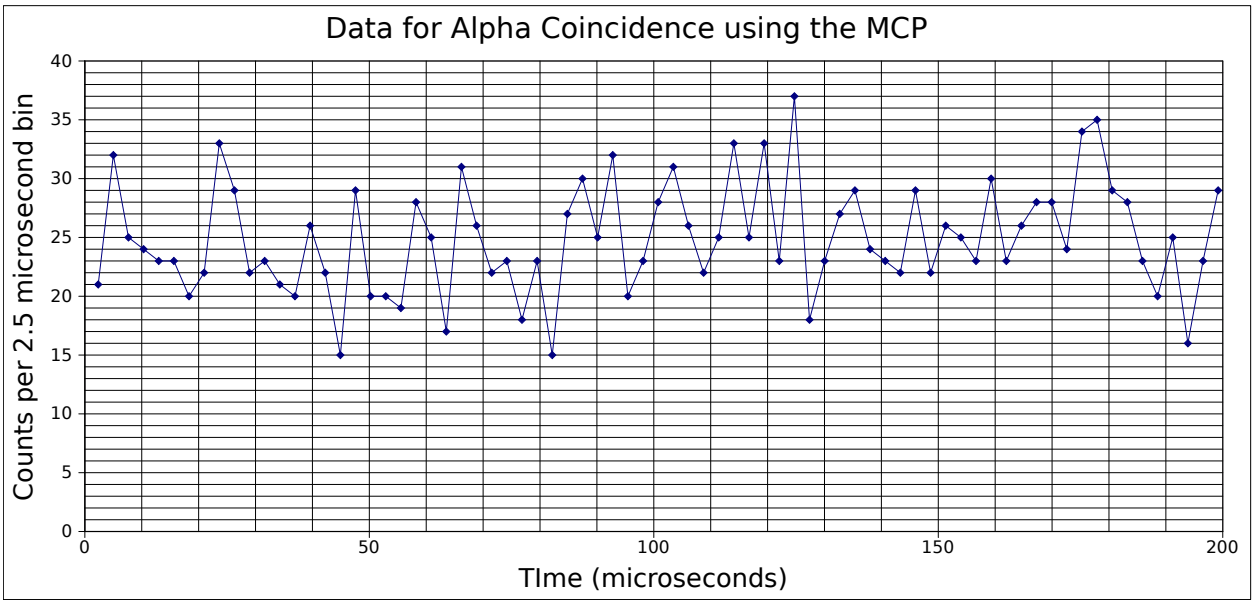

Figure 4.12: This is data used for the alpha coincidence measurement using the MCP. The MCP itself was used as the catcher. The data are in 2.5 μs bins. For this data set, the first μs was vetoed to ignore signals from recoiling nuclei.

becomes

$$\mathrm{ICR} = \mathrm{N} \cdot \lambda \cdot \mathrm{BR}_{\mathrm{iso}} \cdot \mathrm{BR} \cdot \eta_{\mathrm{det}} \tag{4.12}$$

where N is the number of αs detected, which should be very nearly the same as the number of recoils collected. This can be compared to Equation 4.11 to see the differences. Essentially $\mathrm{N}\lambda$ replaces $\mathrm{A}(^{233}\mathrm{U})(\eta_{\mathrm{recoil}})(1\text{-}\mathrm{e}^{-\lambda t})$. Since the N recoils are never present at one time, it's not a true count rate. If it is assumed that the N recoils were all collected at t=0, then this is the count rate that would result. It is useful to perform the calculations this way to maintain the similarities to the previous arrangements.

In the alpha coincidence measurements, the MCP was used as the catcher as well as the detector. Several different time scales were used. With the full scale at 200 ns, the measurement was complete before the recoil arrives. This allowed measurements of the shortest half lives. With the full scale at 2 μs the recoil arrival was clearly evident, and in fact greatly reduced the number of events afterwards. To avoid this problem, the TAC stop signal was vetoed until 600 ns, thus ignoring the recoil signals. This reduces the sensitivity to short half lives, but still allows reasonable sensitivity. Measurements were also made with full scales of 20, 200, and 2000 μs. These all started after 1 μs to avoid the recoils. Figure 4.12 shows the data used for the 200 μs measurement.

The detector efficiency, η_{e^-}, was estimated using $^{235\mathrm{m}}$U. The ^{239}Pu source was 5.38 μCi, 2 inches in diameter, and 1 inch from the 13 mm diameter MCP. The recoil escape fraction is

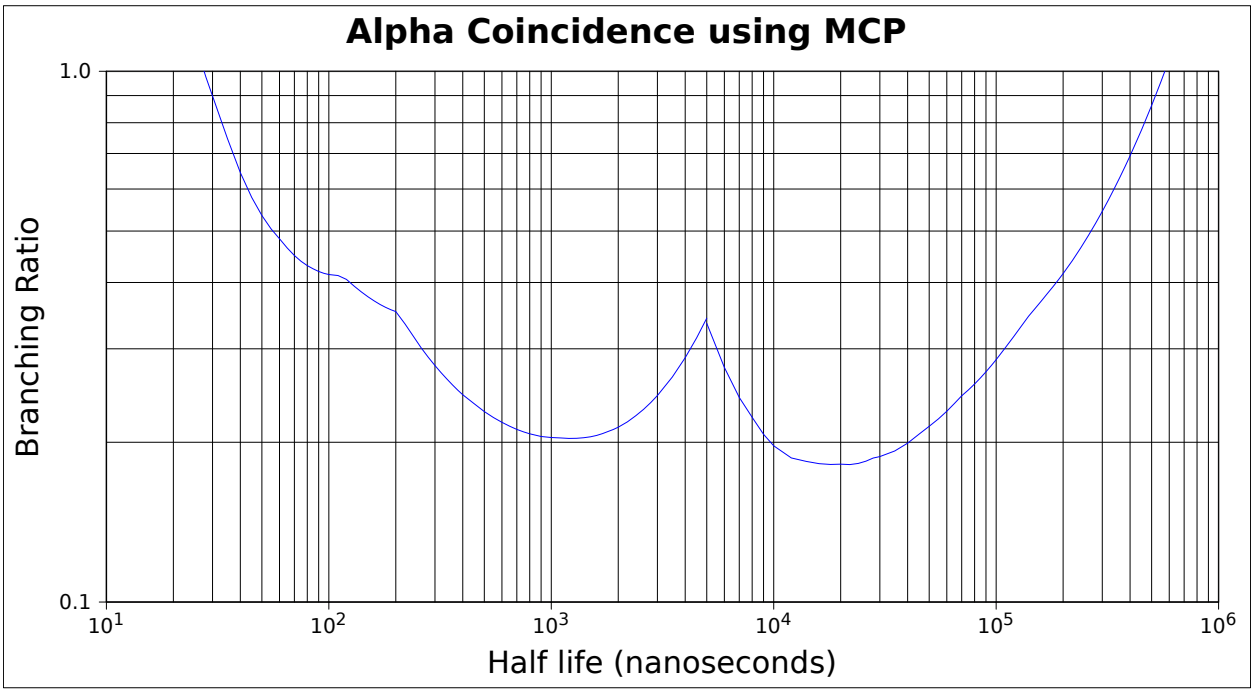

Figure 4.13: This shows the alpha coincidence results using the MCP with recoils collecting directly on the MCP. Five different measurements were made, the only difference being the full scale time of the TAC.

43%, yielding 85,500 recoils per second escaping the surface. The geometric collection onto the MCP is 0.0655, due mainly to its much smaller size than the source. This yields 5600 recoils per second collecting on the MCP. The collection time was only 33 minutes, resulting in 57% of equilibrium decay on the MCP. Therefore 3190 Bq of ^{235m}U were initially on the MCP. The initial count rate was 27 cps, so $\eta_{e^-} = 0.85\%$. Combining η_{e^-} with the number of α particles and the various half lives yields the results that appear in Figure 4.13.

The α coincidence measurement was also performed with the PMT. There was a MgF_2 catcher in front of the PMT. The data for the 20 μs measurement is shown in Figure 4.14. The geometric efficiency used was 40% and the quantum efficiency used was 10%, for a detector efficiency of 4%. Three time scales were used. The first was 200 ns, to measure before the arrival of the recoil. The other two were 20 us and 500 us. The rest of the analysis is the same as for the MCP. The results are shown in Figure 4.15. The very short end of the PMT exclusion plot should be used with a little caution. While efforts were made to have very accurate timing, the jitter in timing from the CFD with the α start signal would probably degrade the measurement below about 10 ns. It is thought the degradation would not be great, but it should be considered.

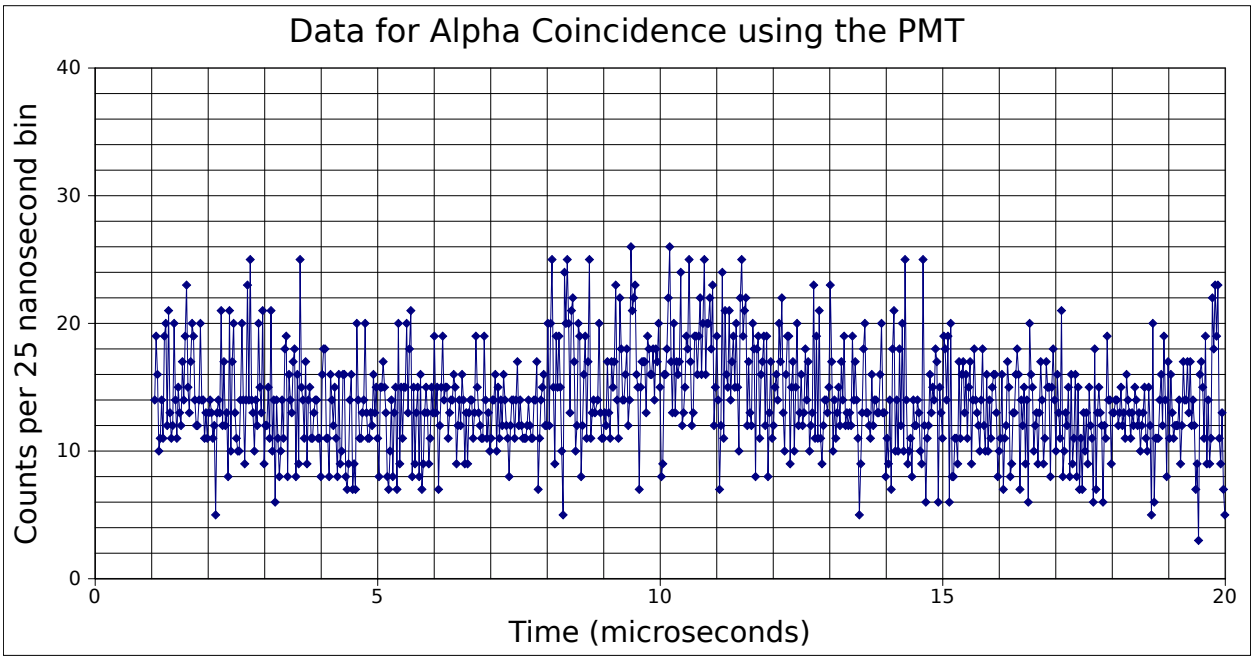

Figure 4.14: This is data used for the alpha coincidence measurement using the PMT. The catcher was MgF_2. The data are in 25 ns bins. For this data set, the first μs was vetoed to ignore signals from recoiling nuclei.

4.5 Results Summary

Combined, these measurements produce an exclusion plot that extends from nanoseconds to days. That's a range that spans over 12 orders of magnitude. Figure 4.16 shows the combined results for the MCP measurements. The MCP measurements were sensitive to times from 30 ns to 200,000 seconds with a small gap around 1 ms. Figure 4.17 shows the combined results for the PMT measurements. The PMT measurements were sensitive to times from about 5 ns to 200,000 seconds, with a larger gap between about 0.1 and 2 ms. No signal was detected from the decay of ^{229m}Th with either the MCP or the PMT.

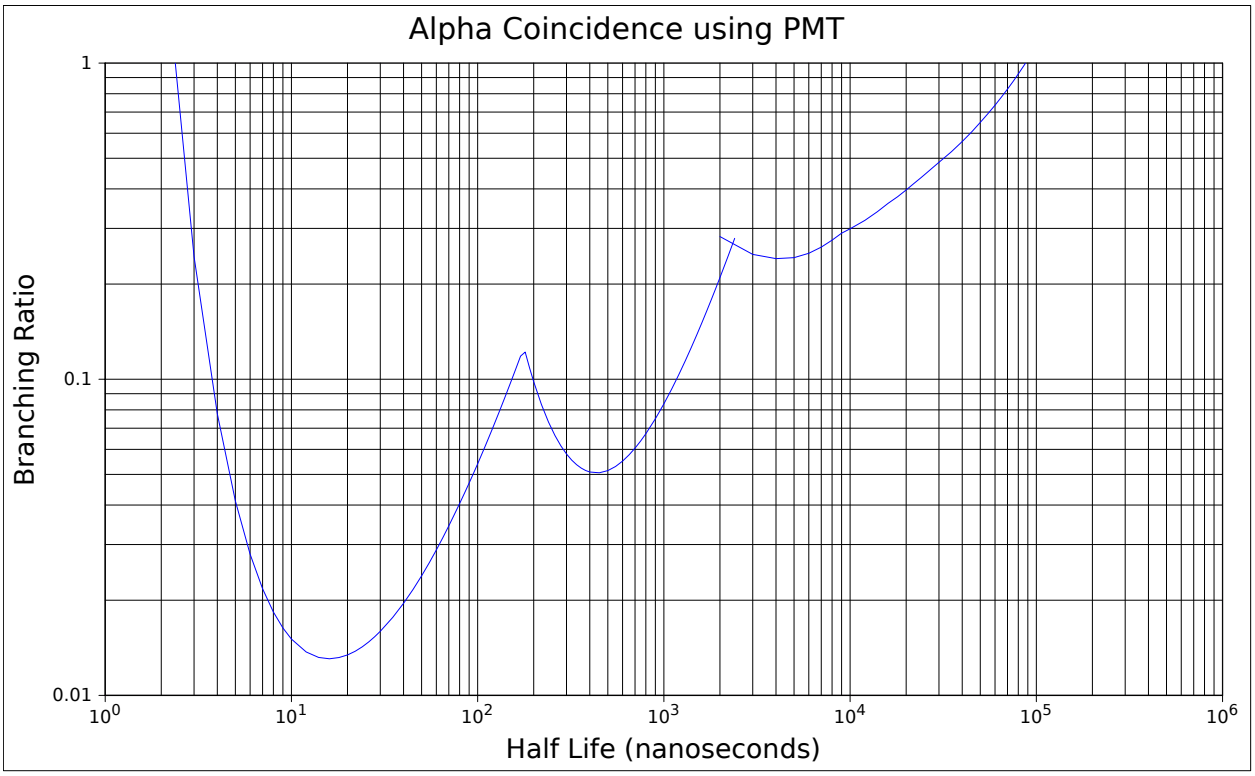

Figure 4.15: This shows the alpha coincidence results using the PMT with a MgF_2 catcher. Three different measurements were made differing only in the full scale time of the TAC.

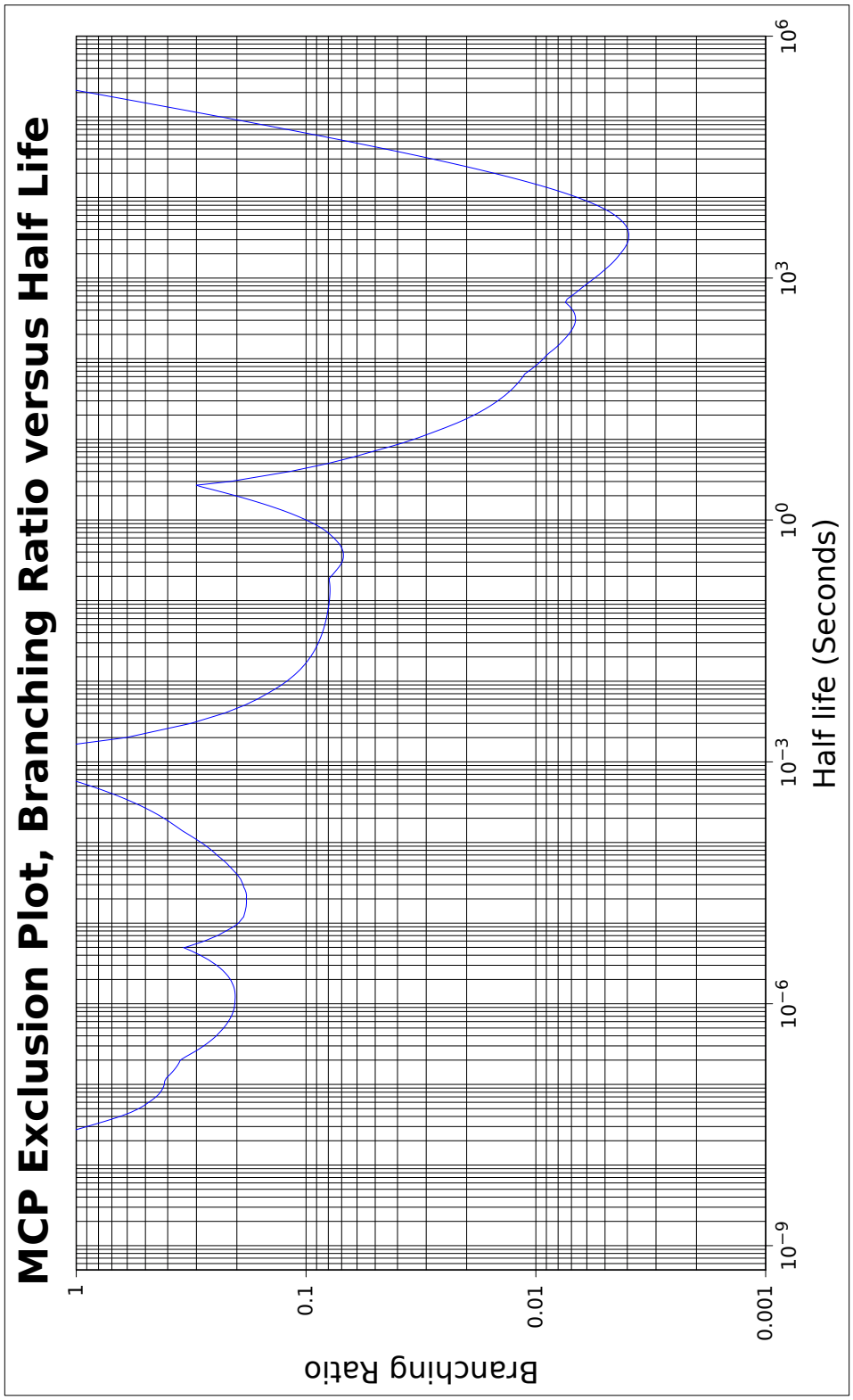

Figure 4.16: This is the summary exclusion plot, combining all data for the MCP.

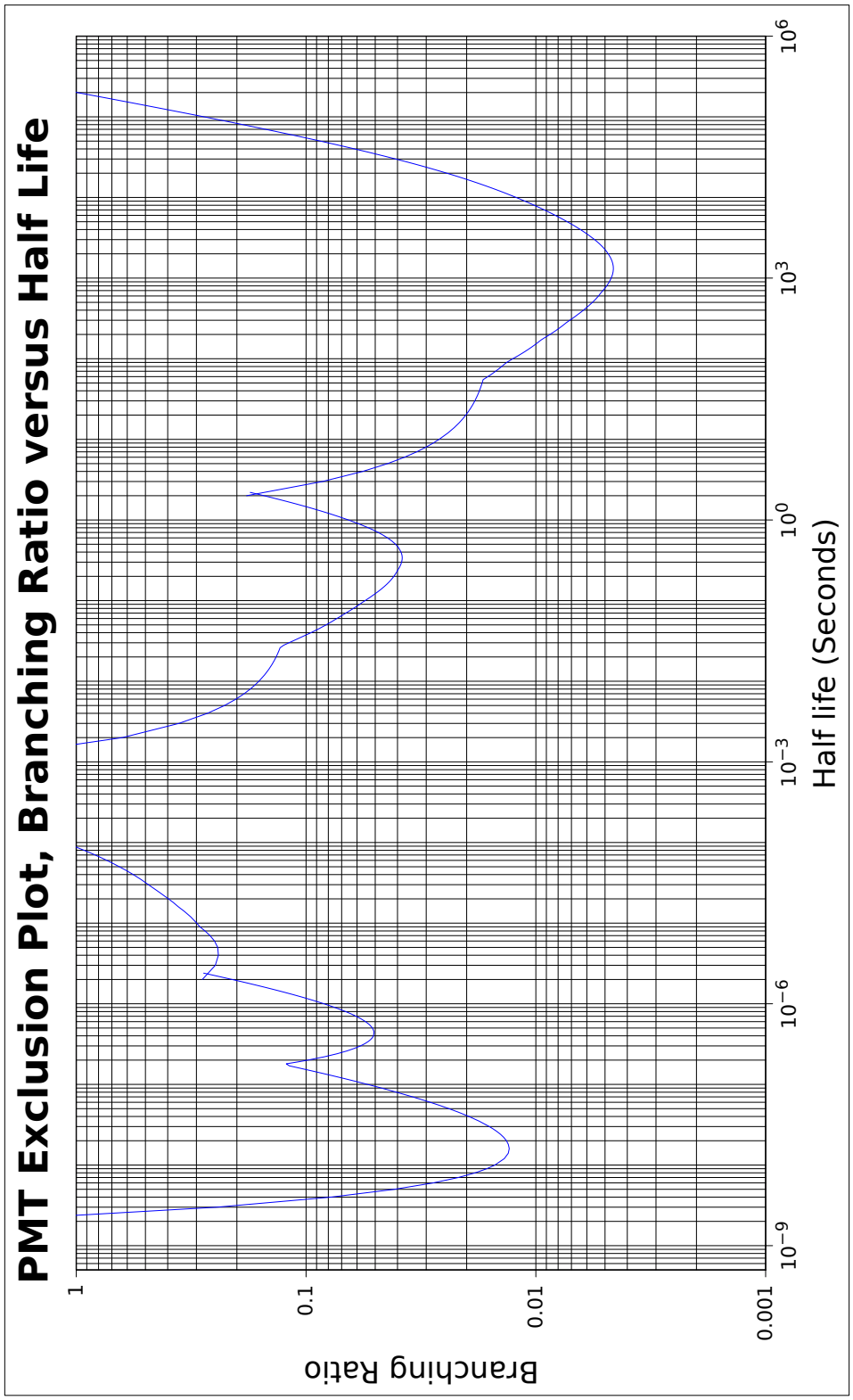

Figure 4.17: This is the summary exclusion plot, combining all data for the PMT.

Chapter 5

Conclusions and Outlook

Despite extensive experimentation, the decay of the isomer was not detected. There are several possible reasons for this. A likely reason is that the isomer decays with a half life that this experiment was not sensitive to. There are several others.

The branching ratio from ^{233}U to the isomer via α decay could be less than expected, making these measurements less sensitive than thought.

It is possible that electrons never escaped from the surface of the various catchers. Since it is not clear how much energy an internal conversion electron would have after decay of ^{229m}Th in a material, it is possible that the energy is below the work function of the catcher. Several means of overcoming this issue were attempted. Catcher materials included low work function elements such as yttrium. Semiconductors were used with the hope that an electron in the conduction band would have a higher probability of escape. As a last resort, the MCP detector itself was used as the catcher in hopes of improved sensitivity.

It is possible the isomer doesn't decay via internal conversion but via γ decay. A PMT sensitive to UV in the region of the spectrum where γ decay of the isomer should occur was used. The PMT was sensitive over the range from 115 to 600 nm, and should have seen light emitted by scintillation or electronic transitions in addition to any γ emission. Some of the catchers used in conjunction with the PMT were transparent over a wide range of wavelengths, including the entire range of the PMT, to increase the probability of detecting any light emitted by buried recoils.

There are several areas where future measurements could be performed. This should be prefaced with a warning: Many things will generate a signal that looks like the decay of the isomer. In this experiment this included a half life that varied from roughly 10 to 15 hours from ^{232}U daughters while using the MCP in the moving catcher arrangement and an 87 ms decay from MgF_2 using the PMT and the mechanical shutter.

The first place for future experiments to search is the time ranges not covered by this experiment. It is unlikely the half life is longer than several hours, both from previous measurements and from theoretical considerations. Another approach is to use different materials, such as a material with a negative electron affinity. These generally have to be

produced in place without exposure to air, making it difficult to obtain. If the isomer could be contained in a ion trap for a sufficiently long time then the γ decay might be observed. Trapping the neutral isomer outside a material would allow the internal conversion electron to be detected. Monitoring the γ or α decay of a freshly prepared sample of ^{229}Th might still yield an answer, despite the several attempts that have already been made. And, of course, it is possible the isomer is decaying via an interaction with an electron from the substrate it is in. If that electron de-excites non-radiatively, then the decay of the isomer would be, in effect, invisible.

Bibliography

[1] B. R. Beck, J. A. Becker, P. Beiersdorfer, G. V. Brown, K. J. Moody, J. B. Wilhelmy, F. S. Porter, C. A. Kilbourne, and R. L. Kelly. Energy splitting of the ground-state doublet in the nucleus ^{229}Th. *Physical Review Letters*, 98, 2007.

[2] B. R. Beck, J. A. Becker, P. Beiersdorfer, G. V. Brown, K. J. Moody, C. Y. Wu, J. B. Wilhelmy, F. S. Porter, C. A. Kilbourne, and R. L. Kelley. Improved value for the energy splitting of the ground-state doublet in the nucleus ^{229}Th. *LLNL-PROC-415170*, 2009.

[3] L. A. Kroger and C. W. Reich. Features of the low-energy level scheme of ^{229}Th as observed in the α-decay of ^{233}U. *Nuclear Physics A*, 259:29–60, 1976.

[4] C. W. Reich and R. G. Helmer. Energy separation of the doublet of intrinsic states at the ground state of ^{229}Th. *Physical Review Letters*, 64(3):271–273, 1990.

[5] D. G. Burke, P. E. Garret, and Tao Qu. Additional evidence for the proposed excited state at$\leq$ 5 eV in ^{229}Th. *Physical Review C*, 42(2), 1990.

[6] R. G. Helmer and C. W. Reich. An excited state of ^{229}Th at 3.5 eV. *Physical Review C*, 49(4), 1994.

[7] G. M. Irwin and K. H. Kim. Observation of electromagnetic radiation from deexcitation of the ^{229}Th isomer. *Physical Review Letters*, 79(6), 1997.

[8] D. S. Richardson, D. M. Benton andD. E. Evans, J. A. R. Griffith, and G. Tungate. Ultraviolet photon emission observed in the search for the decay of the ^{229}Th isomer. *Physical Review Letters*, 80(15), 1998.

[9] S. B. Utter, P. Beiersdorfer, A. Barnes, R. W. Lougheed, J. R. Crespo Lopez-Urrutia, J. A. Becker, and M. S. Weiss. Reexamination of the optical gamma ray decay in ^{229}Th. *Physical Review Letters*, 82(3), 1999.

[10] R. W. Shaw, J. P. Young, S. P. Cooper, and O. F. Webb. Spontaneous ultraviolet emission from ^{233}uranium/^{229}thorium samples. *Physical Review Letters*, 82(6), 1999.

[11] V. Barci, G. Ardisson, G. Garci-Funel, B. Weiss, O. El Samad, and R. K. Sheline. Nuclear structure of ^{229}Th from γ-ray spectroscopy study of ^{233}U α-particle decay. *Physical Review C*, 68(034329), 2003.

[12] Z. O. Guimaraes-Filho and O. Helene. Energy of the $3/2^+$ state of ^{229}Th reexamined. *Physical Review C*, 71, 2005.

[13] S. L. Sakharov. On the energy of the 3.5-ev level in ^{229}Th. *Physics of Atomic Nuclei*, 73(1):1–8, 2009.

[14] E. Browne, E. B. Norman, R. D. Canaan, D. C. Glasgow, J. M. Keller, and J. P. Young. Search for decay of the 3.5-eV level in ^{229}Th. *Physical Review C*, 64(014311), 2001.

[15] T. Mitsugashira, M. Hara, T. Ohtsuki, H. Yuki, K. Takamiya, Y. Kasamatsu, A. Shinohara, H. Kikunaga, and T. Nakanishi. Alpha-decay from the 3.5 ev isomer of ^{229}Th. *Journal of Radioanalytical and Nuclear Chemistry*, 255(1):63–66, 2003.

[16] H. Kikunaga, Y. Kasamatsu, K. Takamiya, T. Mitsugashira, M. Hara, T. Ohtsuki, H. Yuki, and A. Shinohara. Search for α-decay of ^{229m}Th produced from ^{229}Ac β-decay following ^{232}Th(γ,p2n) reaction. *Radiochim. Acta*, 93:507–510, 2005.

[17] I. D. Moore, I. Ahmad, K. Bailey, D. L. Bowers, Z.-T. Lu, T. P. O'Connor, and Z. Yin. Search for a low-lying 3.5 ev isomeric state in ^{229}Th. *Argonne National Laboratory Physics Division Report*, PHY-10990-ME-2004, 2004.

[18] Y. Kasamatsu, H. Kikunaga, K. Takamiya, T. Mitsugashira, T. Nakanishi, Y. Ohkubo, T. Ohtsuki, W. Sato, and A. Shinohara. Search for the decay of ^{229m}Th by photon detection. *Radiochim. Acta*, 93:511–514, 2005.

[19] T. T. Inamura and H. Haba. Search for a "3.5-ev isomer" in ^{229}Th in a hollow-cathode electric discharge. *Physical Review C*, 79(034313), 2009.

[20] H. Kikunaga, Y. Kasasmatsu, H. Haba, T. Mitsugashira, M Hara, K. Takamiya, T. Ohtsuki, A. Yokoyama, T. Nakanishi, and A. Shinohara. Half-life estimation of the first excited state of ^{229}Th by using α-particle spectrometry. *Physical Review C*, 80(034315), 2009.

[21] Xinxin Zhao, Yenny Natali Martinez de Escobar, Robert Rundberg, Evelyn M. Bond, Allen Moody, and David J. Vieira. Observation of the deexcitation of the ^{229m}th nuclear isomer. *Physical Review Letters*, 109(160801), 2012.

[22] A. M. Dykhne and E. V. Tkalya. ^{229m}Th($3/2^+$, 3.5 ev) and a check of the exponentiality of the decay law. *Journal of Experimental and Theoretical Physics Letters*, 67(8), 1998.

[23] E. V. Tkalya. Proposal for a nuclear gamma-ray laser of optical range. *Physical Review Letters*, 106(16), 2011.

[24] V. S. Aleksandrov, Yu. G. Zakharenko, N. A. Kononova, N. A. Mel'nikov, A. A. Pasternak, V. L. Fedorin, L. A. Kharitonov, and K. V. Chekirda. Fundamental problems in metrology. *Measurement Techniques*, 50(12), 2007.

[25] J. C. Berengut, V. A. Dzuba, V. V. Flambaum, and S. G. Porsev. Proposed experimental method to determine α sensitivity of splitting between ground and 7.6 ev isomeric states in ^{229}Th. *Physical Review Letters*, 102(21), 2009.

[26] Wade G. Rellergert, D. DeMille, R. R. Greco, M. P. Hehlen, J. R. Torgerson, and Eric R. Hudson. Constraining the evolution of the fundamental constants with a solid-state optical frequency reference based on the ^{229}Th nucleus. *Physical Review Letters*, 104(20), 2010.

[27] A. C. Hayes, J. L. Friar, and P. Möller. Splitting sensitivity of the ground and 7.6 ev isomeric states of ^{229}Th. *Physical Review C*, 78(2), 2008.

[28] F. F. Karpeshin, I. M. Basnd, M. B. Trzhaskovskaya, and A. Pastor. On the question of electron bridge fro the 3.5-ev isomer of ^{229}Th. *Physical Review Letters*, 83(5), 1999.

[29] Péter Kálmaán and Tamás Bükki. Deexcitation of ^{229}Th^m: Direct γ decay and electronic-bridge process. *Physical Review C*, 63(2), 2001.

[30] E. V. Tkalya. Nonradiative decay of the low-lying nuclear isomer ^{229m}Th(3.5 ev) in a metal. *Journal of Experimental and Theoretical Physics Letters*, 70(6), 1999.

[31] E. V. Tkalya. Excitation of low-lying isomer level of the nucleus ^{229}Th by optical photons. *Journal of Experimental and Theoretical Physics Letters*, 55(4), 1992.

[32] S. G. Porsev, V. V. Flambaum, E. Peik, and Chr. Tamm. Excitation of the isomeric ^{229m}Th nuclear state via an electronic bridge process in ^{229}Th$^+$. *Physical Review Letters*, 105(18), 2010.

[33] F. F. Karpeshin and M. B. Trzhaskovskaya. Impact of the electron environment on the lifetime of the ^{229}Th^m low-lying isomer. *Physical Review C*, 76(5), 2007.

[34] E. Ruchowska, W. A. Plociennik, J. Zylicz, H. Mach, J. Kvasil, A. Algora, N. Amzal, T. Back, M. G. Borge, R. Boutami, P. A. Butler, J. Cederkall, B. Cederwall, B. Fogelberg, L. M. Fraile, H. O. U. Fynbo, E. Hagebo, P. Hoff, H. Gausemel, A. Jungclaus, R. Kaczarowski, A. Kerek, W. Kurcewics, K. Lagergren, E. Nacher, B. Rubio, A. Syntfeld, O. Tengblad, A. A. Wasilewski, and L. Weissman. Nuclear structure of ^{229}Th. *Physical Review C*, 73(4), 2006.

[35] Kenneth S. Krane. *Introductory Nuclear Physics.* John Wiley and Sons, New York, 1988.

[36] Stanley G. Prussin. *Nuclear Physics for Applications.* Wiley-VCH Verlag, Weinheim, Germany, 2007.

[37] S.Y.F. Chu, L.P. Ekstrm, and R.B. Firestone. Retrieved ie.lbl.gov/toipdf/nilsson.pdf, November 2011.

[38] S. Gerstenkorn, P. Luc, J. Verges, D. W. Englekemeir, J. E. Gindler, and F. S. Tomkins. Structures hyperfines du spectre d'etincelle, moment magnetique et quadrupolaire de l'isotope 229 du thorium. *Le Journal de Physique*, 34:483–495, 1974.

[39] Shin Ito and Nobuhiro Maeda. Charge distributions of alpha-recoil atoms from electrodeposited ^{210}Po source. *Nuclear Instruments and Methods in Physics Research*, pages 331–335, 1987.

[40] K. Gunter, F. Asaro, and A. C. Helmholz. Charge and energy distributions of recoils from Th^{226} alpha decay. *Physical Review Letters*, 16(9):362–364, 1966.

[41] T. Carreyre, M. R. Harston, M. Aiche, F. Bourgine, J. F. Chemin, G. Claverie, J. P. Goudour, J. N. Scheurer, F. Attallah, G. Gogaert, J. Kiener, A. Lefebvre, J. Durrell, J. P. Grandin, W. E. Meyerhof, and W. Philips. First direct proof of internal conversion between bound states. *Physical Review C*, 62(2), 2000.

[42] M. Chen. Personal Communication, October 2009.

[43] M. Nève de Mévergnies. Perturbation of the ^{235m}U decay rate by implantation in transition metals. *Physical Review Letters*, 29(17):1188–1191, 1972.

[44] M. Nève de Mévergnies. Chemical effect on the half-life of U^{235m}. *Phyiscal Review Letters*, 23(8):422–425, 1969.

[45] M. Nève de Mévergnies and P. Del Marmol. Effect of the oxidation state on the half-life of ^{235}U^{m}. *Physics Letters*, 49B(5):428–430, 1974.

[46] J. F. Ziegler. *The Stopping and Range of Ions in Matter, volumes 2 to 6.* Pergamon Press, 1977-1985. See also srim.org.

[47] G. W. Fraser. The electron detection efficiency of microchannel plates. *Nuclear Instruments and Methods*, pages 445–449, 1983.

[48] David R. Lide (ed). *CRC Handbook of Chemistry and Physics, 84th Edition.* CRC Press, Boc a Raton, Florida, 2003.

[49] David R. Lide (ed). *CRC Handbook of Chemistry and Physics, 89th Edition.* CRC Press, Boc a Raton, Florida, 2008.

[50] G. W. Gobeli and F. G. Allen. Photoelectric properties of cleaved gaas, gasb, inas, and insb surfaces; comparison with si and ge. *Physical Review*, 137(1A):A245–A254, 1965.

[51] Ben G. Streetman and Sanjay Banerjee. *Solid State Electronic Devices, 5th ed.* Prentice Hall, New Jersey, 2000.

[52] John Robertson. Band offsets of wide-band-gap oxides and implications for future electronic devices. *Journal of Vacuum Science and Technology B*, 18(3):1785–1791, 2000.

[53] Lloyd A. Currie. Limits for qualitative detection and quantitative determination - application to radiochemistry. *Analytical Chemistry*, 40(3):586–593, 1968.